Journal of Asian Earth Sciences 113 (2015) 1117–1131

Contents lists available at ScienceDirect

Journal of Asian Earth Sciences

journal homepage: www.elsevier.com/locate/jseaes

Variations of trace element concentration of magnetite and ilmenite from the Taihe layered intrusion, Emeishan large igneous province, SW China: Implications for magmatic fractionation and origin of Fe–Ti–V oxide ore deposits

Yu-Wei She [a,b], Xie-Yan Song [a,*], Song-Yue Yu [a], Hai-Long He [a,b]

[a] State Key Laboratory of Ore Deposit Geochemistry, Institute of Geochemistry, Chinese Academy of Sciences, Guiyang 550002, China
[b] University of Chinese Academy of Sciences, Beijing 100049, China

ARTICLE INFO

Article history:
Received 17 October 2014
Received in revised form 16 March 2015
Accepted 17 March 2015
Available online 24 March 2015

Keywords:
Trace elements
Magnetite
Ilmenite
Fe–Ti–V oxide deposit
Fractional crystallization
Taihe
Emeishan large igneous province

ABSTRACT

In situ LA–ICP–MS trace elemental analysis has been applied to magnetite and ilmenite of the Taihe layered intrusion, Emeishan large igneous province, SW China, in order to understand better fractionation processes of magma and origin of Fe–Ti–V oxide ore deposits. The periodic reversals in Mg, Ti, Mn in magnetite and Mg, Sc in ilmenite are found in the Middle Zone of the intrusion and agree with fractionation trends as recorded by olivine (Fo), plagioclase (An) and clinopyroxene (Mg#) compositions. These suggest the Taihe intrusion formed from open magma chamber processes in a magma conduit with multiple replenishments of more primitive magmas. The V and Cr of magnetite are well correlated with V and Cr of clinopyroxene indicating that they became liquidus phases almost simultaneously at an early stage of magma evolution. Ilmenite from the Middle and Upper Zones shows variable Cr, Ni, V, Mg, Nb, Ta and Sc contents indicating that ilmenite at some stratigraphic levels crystallized slightly earlier than magnetite and clinopyroxene. The early crystallization of magnetite and ilmenite is the result of the high FeO_t and TiO_2 contents in the parental magma. The ilmenite crystallization before magnetite in the Middle and Upper Zones can be attributed to higher TiO_2 content of the magma due to the remelting of pre-existing ilmenite in a middle-level magma chamber. Compared to the coeval high-Ti basalts, the relatively low Zr, Hf, Nb and Ta contents in both magnetite and ilmenite throughout the Taihe intrusion indicate that they crystallized from Fe–Ti–(P)-rich silicate magmas. Positive correlations of Ti with Mg, Mn, Sc and Zr of magnetite, and Zr with Sc, Hf and Nb of ilmenite also suggest that magnetite and ilmenite crystallized continuously from the homogeneous silicate magma rather than an immiscible Fe-rich melt. Therefore, frequent replenishments of Fe–Ti–(P)-rich silicate magma and gravitational sorting and settling are crucial for the formation the massive and apatite-rich disseminated ores in the Lower and Middle Zones of the Taihe intrusion.

1. Introduction

Magnetite and ilmenite are two common minerals in igneous, metamorphic and sedimentary rocks. In particular, they are major ore minerals in many hydrothermal iron deposits, banded iron formation, and magmatic Fe–Ti–V and Fe–Ti–P ore deposits (Dupuis and Beaudoin, 2011; Dare et al., 2014; Nadoll et al., 2014). Recently, a number of studies focus on trace element compositions of magnetite by LA–ICP–MS analysis (e.g. Dare et al., 2012, 2014; Huang et al., 2013; Nadoll et al., 2012, 2014). Because trace elements are sensitive to different conditions, the trace element features of magnetite can be an important indicator of petrogenetic and provenance (Dare et al., 2014; Nadoll et al., 2014). Trace element compositions of ilmenite, although less commonly reported (e.g. Charlier et al., 2007; Jang and Naslund, 2003), may be another excellent monitor of crystallization and ore-forming processes because it contains a large number of minor and trace elements such as Mn, Mg, V, Cr, Ni, Sc, Nb, Ta, Zr and Hf (Jang and Naslund, 2003; Dare et al., 2012).

The Taihe intrusion is one of the layered mafic–ultramafic intrusions hosting giant Fe–Ti–V oxide deposits in the central zone of

* Corresponding author at: State Key Laboratory of Ore Deposit Geochemistry, Institute of Geochemistry, Chinese Academy of Sciences, 46th Guanshui Road, Guiyang 550002, China. Tel.: +86 0851 5895538; fax: +86 0851 5891664.
E-mail address: songxieyan@vip.gyig.ac.cn (X.-Y. Song).

http://dx.doi.org/10.1016/j.jseaes.2015.03.029
1367-9120/

the Emeishan large igneous province (ELIP), in SW China. The Lower Zone of the intrusion comprising massive Fe–Ti–V oxide ores and (olivine) gabbro represents the crystallization products of Fe–Ti enriched parental magma (Hou et al., 2012; Shellnutt et al., 2011). The apatite-rich disseminated Fe–Ti–V oxide ore layers with thicknesses of 15–100 m forming the lower parts of cyclic units of the Middle Zone indicate a Fe–Ti–P enriched magma (She et al., 2014a,b). Previous studies suggested that a Fe–Ti enriched parental magma of the Lower Zone was produced by the Emeishan high-Ti picritic magma via extensive fractionation of silicate minerals at a deep-seated magma chamber (She et al., 2014a; Hou et al., 2012; Shellnutt et al., 2011). The Fe–Ti–P enriched parental magma of the Middle Zone was produced by mixing of Fe–Ti enriched magma from depth and an evolved P saturated magma in a middle-level magma chamber as well as partial remelting of pre-existing fusible minerals (She et al., 2014a,b). However, the effect of magma mixing and remelting of minerals on the trace element compositions of magnetite and ilmenite has not been addressed. Moreover, crystallization of either of magnetite and ilmenite may have a significant effect on the trace element partitioning into the other mineral during differentiation of magma. Although recent study provides trace element data of magnetite, by LA–ICP–MS, from other Fe–Ti–V deposits in the Emeishan LIP (Liu et al., 2014a,b), only three samples have been analysed from the Taihe from which it is difficult to interpret magma chamber processes. Furthermore, magmatic ilmenite from the Fe–Ti oxide ore deposits of ELIP has not been analyzed by LA–ICP–MS.

In this study, trace element compositions of magnetite and ilmenite of the Taihe intrusion are measured using LA–ICP–MS to investigate the fractional crystallization history and origin of Fe–Ti–V oxide deposit of the Taihe intrusion. Our results suggest that most of the magnetite and ilmenite crystallized together with mafic silicates at an early stage of magma differentiation. Ilmenite from some stratigraphic levels of the Middle and Upper Zones crystallized earlier than magnetite and clinopyroxene. Early crystallization of Fe–Ti oxides is the result of the high FeO_t and TiO_2 contents in the parental magmas. The gravitational sorting and settling of magnetite and ilmenite result in formation of Fe–Ti–V oxide ore layers.

2. Geology background

The ELIP lies to the western margin of the Yangtze Block and the eastern margin of the Tibetan Plateau, and consists of flood basalts, mafic–ultramafic intrusions and felsic plutons (Fig. 1). The Emeishan flood basalts cover an area of more than 5×10^5 km^2, which are mainly exposed in the Sichuan, Guizhou and Yunnan Provinces (Xu et al., 2001; Song et al., 2001, 2008, 2009; Ali

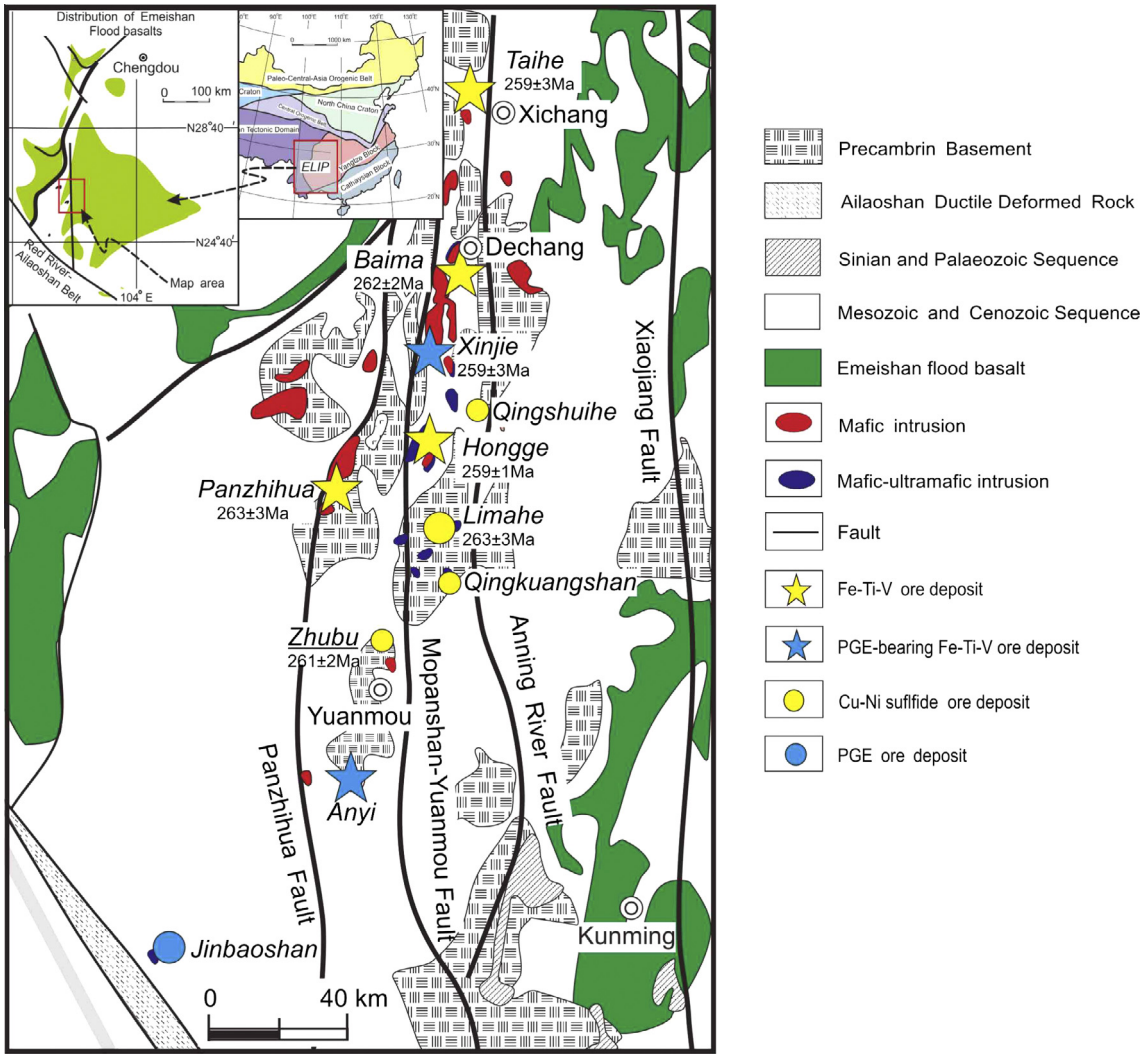

Fig. 1. Regional geological map of the central part of the Emeishan Large Igneous Province and locations of the mafic–ultramafic intrusions hosting Fe–Ti oxide deposit and magmatic sulfide deposits.

et al., 2005; Shellnutt, 2014). The intrusions including large and small layered mafic–ultramafic intrusions are economically important due to the occurrence of Cu–Ni–(PGE) sulfide deposits and Fe–Ti–V oxide deposits (Zhou et al., 2002; Zhong et al., 2002; Zhang et al., 2009; Tao et al., 2008). They are the result of mantle plume-related magmatism in the Late Permian at ~260 Ma based on trace element and Sr–Nd isotopes of the intrusions and Emeishan flood basalts (Chung and Jahn, 1995; Zhang et al., 2006; Kamenetsky et al., 2012).

In the central part of ELIP (known as Pan-Xi region), the Fe–Ti oxide ore-bearing layered mafic–ultramafic intrusions are distributed along a series of N–S trending faults and include the Panzhihua (263 ± 3 Ma, Zhou et al., 2005; Shellnutt et al., 2012), Hongge (259 ± 1 Ma, Zhong and Zhu, 2006), Baima (262 ± 3 Ma, Zhou et al., 2008; Shellnutt et al., 2009) and Taihe intrusions (259 ± 3 Ma, She et al., 2014a) (Fig. 1). These mafic–ultramafic intrusions are characterized by well-developed igneous layering and cyclic units within the intrusions. The Panzhihua and Baima intrusions are mafic throughout and have stratiform Fe–Ti oxide ore bodies in the Lower Zone of the intrusions (Panzhihua: 1333 Mt ore with ~33% total Fe, ~12% TiO_2 and ~0.3% V_2O_5 and Baima: 1497 Mt ore with ~26% total Fe, ~7% TiO_2 and ~0.21% V_2O_5). The Hongge and Taihe intrusions contain ultramafic portions, and the main Fe–Ti–V oxide ore layers occur in both the Lower and Middle Zones of the intrusions (Hongge: 4572 Mt ore with ~27% total Fe, ~11% TiO_2 and ~0.24% V_2O_5 and Taihe: 810 Mt ore with ~33% total Fe, ~12% TiO_2 and ~0.3% V_2O_5) (Ma et al., 2003).

3. The Taihe intrusion and petrography

The Taihe intrusion is approximately 3 km long and 2 km wide, with an exposed area of ~13 km^2 (Fig. 2). The layering dips to the southeast with angles of 50–60° and the intrusive body has a thickness of ~1.2 km. The Taihe intrusion is completely surrounded by a contemporaneous syenite pluton and some syenite dykes, with thicknesses of several meters, intrude the intrusion suggesting that the syenite formed slightly later (She et al., 2014a; Shellnutt et al., 2010, 2011; Hou et al., 2012; Pang et al., 2010). Based on mineral assemblages and lithologic textures, the Taihe intrusion can be divided into Lower Zone, Middle Zone and Upper Zone (She et al., 2014a,b) (Fig. 2).

The Lower Zone is comprised of olivine clinopyroxenite, (olivine) gabbro and ~60 m thick massive Fe–Ti–V oxide ores, from the base to the top (Fig. 2). The olivine clinopyroxenite contains ~65 modal% clinopyroxene, ~20% olivine, and minor Fe–Ti oxides (<10%) and plagioclase (<5%) and interstitial hornblende (<2%). As plagioclase increases to more than 50%, the rock changes to (olivine) gabbro. The massive Fe–Ti–V oxide ores are composed chiefly of Fe–Ti oxides (50–90%) and clinopyroxene (10–50%) with minor interstitial hornblende (<2%). These rocks are medium to coarse-grained and display orthocumulate textures without a prominent layered structure. The Fe–Ti oxide assemblages in the Lower Zone rocks are dominated by magnetite over ilmenite (Ilmenite/Magnetite = 0.25–0.5). Some Fe–Ti oxide crystals are enclosed in the olivine or clinopyroxene (Fig. 3a and b). Magnetite and ilmenite are polygonal or irregular crystals,

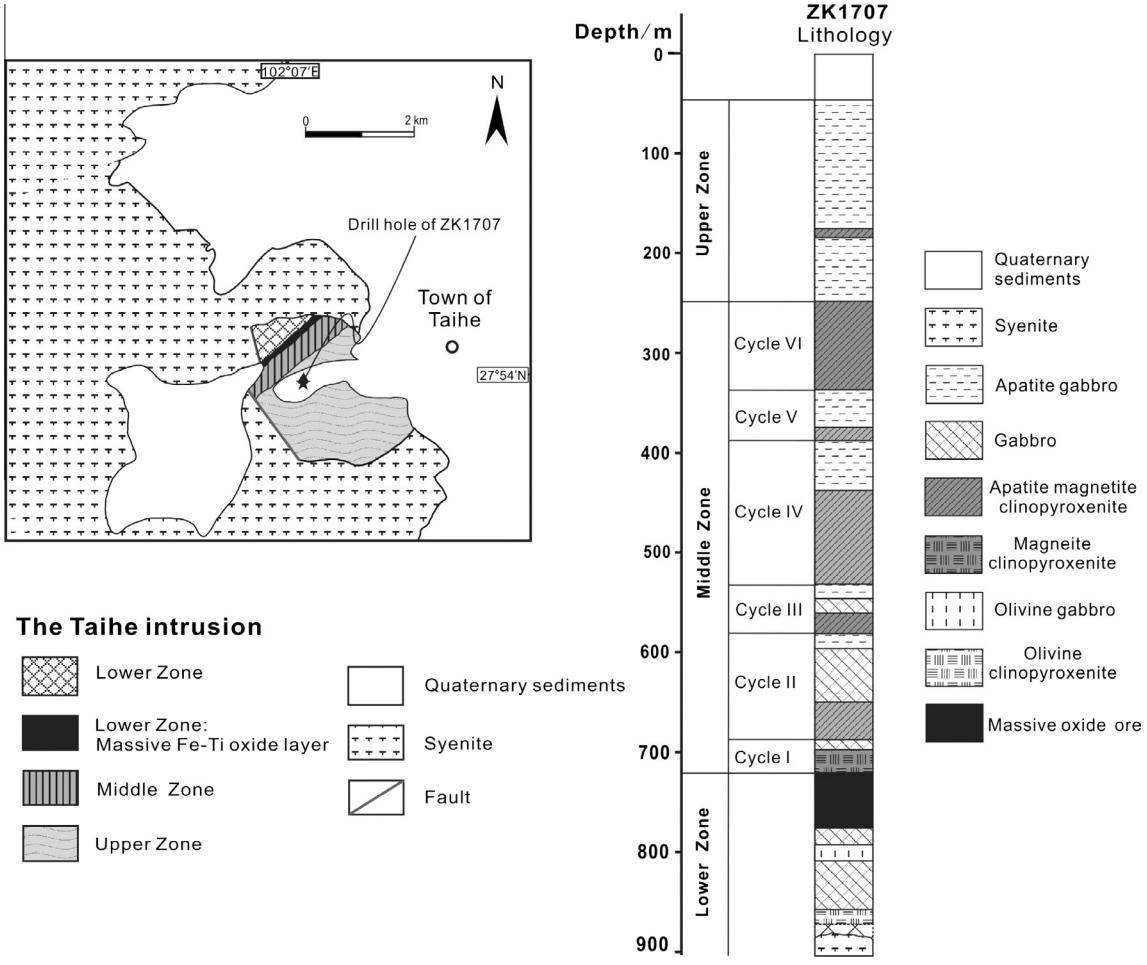

Fig. 2. Simplified geological map of the Taihe layered intrusion and the stratigraphic column of the drill-core of ZK1707.

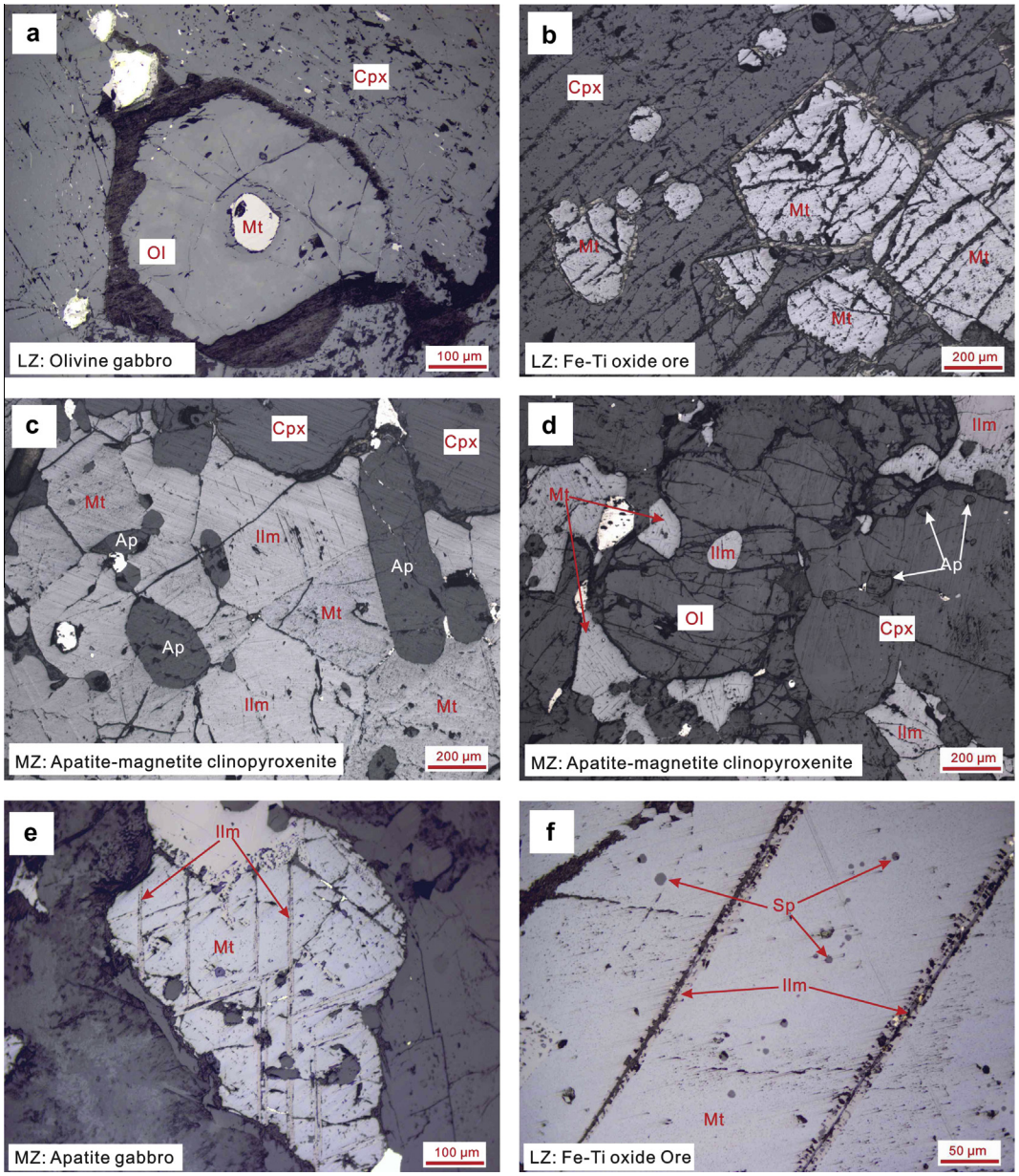

Fig. 3. Microscope photos under reflected light showing typical rock textures of the Taihe intrusion. (a) Magnetite inclusion enclosed in olivine in the olivine gabbro of the Lower Zone; (b) Subhedral–euhedral magnetite crystals enclosed in coarse-grained clinopyroxene in the Fe–Ti oxide ore of the Lower Zone; (c) Abundant magnetite and ilmenite associated with subhedal–euhedal apatite in the apatite–magnetite clinopyroxenite of the Middle Zone; (d) Ilmenite inclusions enclosed in olivine in the apatite–magnetite clinopryxoenite of the Middle Zone; (e) Internal textures of magnetite of the apatite gabbro of the Middle Zone showing the exsolutions of ilmenite lamellae; (f) Internal textures of magnetite of the massive Fe–Ti oxide ore of the Lower Zone showing the exsolution of ilmenite lamellae and granular spinel. LZ = Lower Zone; MZ = Middle Zone; UZ = Upper Zone; Ol = Olivine; Pl = Plagioclase; Cpx = Clinopyroxene; Mt = Magnetite; Ilm = Ilmenite; Ap = Apatite.

0.5–1 mm in diameter, and magnetite contains commonly contains abundant trellis ilmenite lamellae (5–10 μm) and small spinel blebs (1–5 μm) (Fig. 3f). Olivine is typically rounded or subrounded and enclosed by subhedral clinopyroxene crystals. Clinopyroxene is usually subhedral to euhedral and has exsolution ilmenite lamellae parallel to its prismatic cleavages. Plagioclase occurs as subhedral to euhedral tabular crystals. Minor hornblende occurs as irregular interstitial grains or the reaction rims surrounding plagioclase and clinopyroxene.

The Lower Zone, has well-developed igneous layering and can be divided into six cyclic units (Cycle I–VI) which consist of apatite-magnetite clinopyroxenite in the lower parts and apatite gabbro in the upper parts (She et al., 2014a,b) (Fig. 2). The layered structure is represented by alternative dark layers rich in mafic silicates and Fe–Ti oxides and light layers rich in plagioclase. These rocks show medium-sized grains relative to that of the Lower Zone. The (apatite)–magnetite clinopyroxenite consists of clinopyroxene (40–70%) and Fe–Ti oxides (20–40%) with varying amounts of apatite (0–12%) and olivine (0–20%), and minor plagioclase (<5%) and hornblende (<2%). The (apatite) gabbro is composed of plagioclase (40–60%) and clinopyroxene (30–50%) with varying amounts of apatite (0–8%) and Fe–Ti oxides (<20%). When apatite decreases to less than 5%, it is named as magnetite clinopyroxenite and gabbro. The Fe–Ti oxides form aggregates and isolated grains set in a matrix of clinopyroxene and olivine. This is because the subsolidus recrystallization of Fe–Ti oxides results in magnetite and ilmenite forming interstitial fillings between the silicate minerals (Pang et al., 2008; Shellnutt et al., 2011). It is noteworthy that the magnetite and ilmenite aggregates are closely associated with cumulus apatite in apatite magnetite clinopyroxenites (Fig. 3c).

The ilmenite/magnetite ratios (0.5–2) of the Middle Zone rocks are higher than that of Lower Zone rocks (Ilm/Mt = 0.25–0.5). Magnetite and ilmenite occur either as small grains enclosed by the mafic silicate minerals (Fig. 3d), or as cumulus layers together with silicate minerals (Fig. 3c). The magnetite grains commonly exhibit a variety of ilmenite exsolutions (Fig. 3e). The clinopyroxene crystals usually display exsolution ilmenite lamellae parallel to its prismatic cleavages.

The Upper Zone is characterized by lower Fe–Ti oxides and higher plagioclase abundances relative to the Middle and Lower Zones. This zone consists mainly of apatite gabbro and a thin interlayer of apatite–magnetite clinopyroxenite (Fig. 2). The apatite gabbro contains coarse-grained plagioclase (50–70%) and medium-grained clinopyroxene (20–40%) with minor apatite (5–8%) and Fe–Ti oxides (<10%). The magnetite and ilmenite are generally interstitial between abundant plagioclase and clinopyroxene (She et al., 2014a,b).

4. Samples and analytical methods

In this study, we chose 35 samples from the drill core of ZK1707 of the Taihe intrusion (Fig. 2) and analyzed trace elements of magnetite and ilmenite grains from the thin sections.

Trace elements in magnetite and ilmenite were determined by a laser ablation inductively coupled-plasma mass spectrometry (LA–ICP–MS) at the State Key Laboratory of Ore Deposit Geochemistry, Institute of Geochemistry, Chinese Academy of Sciences, using a GeoLasPro laser-ablation system. Ion-signal intensities were acquired through an Agilent 7700x ICP-MS instrument with Helium (He) as the carrier gas. Ablation protocol employed a spot diameter of 60 μm at 6 Hz repetition rate for 40 s (equating to 240 pulses) in this study. Each analysis incorporated a background acquisition for approximately 20 s (gas blank) followed by 40s of data acquisition. We used ^{57}Fe as the internal standard, and the details of analytical methods are available in Dare et al. (2012). The samples that the total content of minor elements in magnetite by the electron microprobe analysis is <3 wt% (She et al., 2014b) are calculated using 69 wt% for the Fe internal standard. In the case of the Ti-rich magnetite, which hosts 6–19 wt% of minor elements, we used 54–66 wt% for the Fe internal standard. The stoichiometric value of 35% for the Fe internal standard is used to calculate the element contents of ilmenite. All data was reduced using an IOLITE software by subtracting gas background from each of the isotopes. USGS standard reference materials, BIR-1G and BHVO-2G, were used to calibrate the LA–ICP–MS and listed in Table 1. A natural magnetite (BC-28) from the Bushveld Complex (Dare et al., 2012) was analysed as an unknown sample to monitor the data quality during LA–ICP–MS analysis. The results of the reference materials are generally within 10% analytical error of recommended values (Table 1). The average compositions of magnetite and ilmenite in each sample are list in Tables 2 and 3, respectively.

5. Analytical results

Although the exsolution of ilmenite and spinel in magnetite is common in the Taihe intrusion, the average compositions of magnetite including exsolution lamellae of ilmenite and spinel can be obtained by the large spot size of LA–ICP–MS analysis. Because the size of the ilmenite exsolutions (5–10 μm) and spinel blebs (<5 μm) within magnetite grains always smaller than that of the laser spot size (60 μm), the LA–ICP–MS results approximate well the original composition of magnetite before subsolidus exsolution. Fig. 4a and b shows that the measured results of the reference materials BIR-1G and BHVO-2G and BC-28 magnetite agree well with recommended values, indicating that the calibration of the LA–ICP–MS produces accurate and precise results (Table 1).

Fig. 5 shows the variation of magnetite and ilmenite composition as a function of height of the Taihe intrusion. In the Lower Zone, Mg, Mn, Ti of magnetite and Mg, Sc of ilmenite show small variations except for one sample (Fig. 5a–e). However, these elements in magnetite and ilmenite show little variation in the massive ore layers of the top of the Lower Zone (Fig. 5a–e). In the Middle Zone, Mn and Ti in magnetite and Mg and Sc in ilmenite decrease regularly from the base to the top of each cyclic unit (except for Cycle I) (Fig. 5b–e). From the Cycle VI of the Middle Zone upwards to the Upper Zone, all magma differentiation indices gradually decrease (Fig. 5a–e).

In order to compare various compositions of magnetite and ilmenite, the elements of Cr, Ni, V, Co, Ti, Mg, Mn, Ga, Nb, Ta, Sc, Hf and Zr were normalized to Emeishan high-Ti basalts in order of their compatibility into magnetite (following Dare et al., 2014) (Fig. 6). The normalized multielement variation diagrams of magnetite from the Lower Zone show high Cr, Ni, V, Co, Ti, Mn and Ga which are compatible into magnetite, and low Zr, Hf, Ta and Nb values, which are incompatible into magnetite (Fig. 6a). The

Table 1
Analyses of reference materials used in the calibration of LA–ICP–MS and to monitor the data quality.

Element		BIR-1G	This study		BHVO-2G	This study		BC-28	This study	
	D.L.	Accepted values	Average (n = 30)	St dev	Accepted values	Average (n = 30)	St dev	Accepted values	Average (n = 30)	St dev
24Mg	2.63	56,400	56,652	1979	42,780	43,878	1483	11,618	12,387	1652
27Al	4.69	82,150	77,633	2415	72,080	70,783	1712	20,787	24,949	3821
45Sc	1.18	43	47	1.8	33	37	2.2	31	24	2.6
47Ti	0.972	5400	5723	101	16,300	17,035	362	87,615	87,855	4777
51V	0.306	326	330	6	308	336	7	9603	11,456	779
52Cr	2.84	392	393	14	293	296	6	1172	1064	128
55Mn	7.67	1741	1337	19	1316	1339	5	2125	2677	219
59Co	0.135	52	51	1.5	44	44	1.3	241	270	32
60Ni	8.35	178	176	9	116	121	5	537	600	54
65Cu	1.55	119	114	5	127	120	4	33	37	49
66Zn	4.42	78	78	2	102	114	5	588	644	134
71Ga	0.055	15	15	1	22	20	1	41.1	53	1.51
88Sr	0.001	109	105	3	396	401	8			
89Y	0.001	14.3	14	0.2	26	25	0.7	0.08	0.12	0.22
90Zr	0.012	14	14	0.6	170	175	9	27.5	20.2	2.65
93Nb	0.011	0.52	0.82	0.42	18.3	16.8	0.58	1.72	1.69	0.19
178Hf	0.008	0.57	0.59	0.08	4.32	4.49	0.24	0.58	0.56	0.36
181Ta	0.002	0.036	0.034	0.01	1.15	1.1	0.07	0.07	0.18	0.16

D.L. = detection limit; St dev = standard deviation. Accepted values for BIR-1G and BHVO-2G are from certificate; accepted values for BC-28 are from Dare et al. (2014).

Table 2
Summary of LA–ICP–MS analyses for compositions of cumulus magnetite and magnetite inclusions enclosed in olivine from the Taihe intrusion.

Sample	ST11-58	ST11-56	ST11-52	ST11-51	ST11-48	ST11-02	ST11-03	ST11-05	ST11-06	ST11-08	ST11-09	ST11-10
Depth/m	81	113	169	173	216	246	270	305	323	363	381	400
Rock	Ap Gab	Ap Gab	Ap Gab	Ap Mt Cpx	Ap Gab	Ap Mt Cpx	Ap Mt Cpx	Mt Cpx	Ap Mt Cpx	Ap Gab	Ap Mt Cpx	Ap Gab
Zone	UZ	UZ	UZ	UZ	UZ	MZ	MZ	MZ	MZ	MZ	MZ	MZ
Cycle						VI	VI	VI	VI	V	V	IV
Number	3	3	3	2	3	3	3	3	3	3	3	3
Minor and trace elements (ppm)												
Ti	1304	17,752	1220	8842	4585	30,172	41,611	3728	17,386	50,697	51,851	14,426
Al	1908	24,197	7313	11,256	24,031	28,519	18,911	5486	17,631	24,533	22,432	17,446
Mn	109	877	118	927	339	2550	3568	615	1682	3262	3721	800
Mg	33	19,249	186	817	272	6400	11,483	702	5318	8112	9406	5173
Sc	0.36	1.98	1.20	0.61	1.17	3.03	4.91	1.34	1.68	3.25	3.65	2.92
V	4493	3729	3432	3570	3956	3850	2762	3424	2800	3699	3616	4270
Cr	14.95	46.29	115.73	66.83	49.33	43.24	34.63	156.67	30.64	86.20	39.37	23.01
Co	7.39	24.33	39.57	36.61	36.64	108.84	41.48	75.95	84.23	53.93	79.48	84.79
Ni	28.92	5.99	12.16	12.87	13.19	7.34	6.07	325.89	6.65	0.30	1.29	7.73
Cu	-0.74	0.57	1.68	2.74	2.66	2.77	406.80	-1.47	3.86	55.93	43.75	1.93
Ga	48.17	13.93	63.50	63.06	115.25	85.16	61.54	78.36	69.63	70.79	71.89	75.18
Sr	0.05	8.79	0.29	3.02	0.39	0.15	0.58	1.24	0.16	1.52	0.48	0.11
Y	0.01	0.71	0.00	0.31	0.00	0.00	0.05	0.00	0.00	0.02	0.08	0.00
Zr	0.01	3.21	0.35	1.43	3.08	1.27	0.83	0.03	0.85	2.30	2.74	1.35
Nb	0.07	0.25	0.00	1.00	0.11	0.00	0.00	0.00	0.02	0.17	0.22	0.04
Hf	0.00	0.06	0.00	0.17	0.05	0.00	0.07	0.00	0.02	0.11	0.07	0.05
Ta	0.00	0.02	0.00	0.21	0.00	0.01	0.02	0.02	0.00	0.05	0.03	0.00

ST11-11	ST11-13	ST11-14	ST11-15	ST11-17	ST11-18	ST11-19	ST11-20	ST11-21	ST11-22	ST11-23	ST11-25
415	443	459	471	506	517	534	558	575	589	602	629
Ap Gab	Ap Mt Cpx	Ap Mt Cpx	Ap Mt Cpx	Ap Mt Cpx	Ap Mt Cpx	Ap Gab	Gab	Ap Mt Cpx	Gab	Gab	Gab
MZ	MZ	MZ	MZ	MZ	MZ	MZ	MZ	MZ	MZ	MZ	MZ
IV	IV	IV	IV	IV	IV	III	III	III	II	II	II
3	3	3	3	3	3	3	3	2	3	3	4
768	63,786	40,384	41,386	35,123	57,660	9062	2022	34,418	30,778	57,431	74,871
2356	18,989	20,299	24,631	29,351	26,256	12,122	13,730	21,323	23,800	24,841	24,896
132	4201	3132	2792	3027	3693	417	224	1147	1492	3259	3966
197	7369	9195	8962	7072	10,812	2375	561	536	8279	9800	7648
1.25	4.13	4.80	3.02	1.98	4.68	1.83	0.99	3.51	2.87	3.17	6.33
3430	3441	3833	3583	4033	3536	4862	4459	4709	4384	4114	4166
66.24	22.37	29.44	28.62	31.59	29.40	45.70	509.34	118.63	71.93	77.93	81.60
23.06	80.15	110.29	104.64	126.76	89.28	63.52	48.16	72.31	93.78	85.96	124.80
14.52	2.54	5.93	3.66	4.01	1.74	10.31	40.84	59.96	48.89	52.57	52.53
1.27	3.40	0.34	1.90	18.07	3.12	3.64	2.10	2.93	0.34	5.98	9.76
53.78	67.57	71.45	75.89	84.18	61.80	71.46	75.83	70.49	81.08	73.10	66.53
0.79	1.91	0.13	1.41	0.08	0.67	1.49	2.22	0.60	0.17	0.01	0.18
0.01	0.00	0.01	0.15	0.00	0.00	0.01	0.01	0.00	0.00	0.00	0.00
0.08	2.74	1.25	2.69	1.21	4.08	0.78	0.69	1.84	1.85	4.54	5.79
0.14	0.18	0.01	0.11	0.01	0.34	0.01	0.00	0.09	0.00	0.11	0.96
0.00	0.06	0.07	0.11	0.04	0.25	0.01	0.00	0.13	0.07	0.15	0.19
0.04	0.03	0.01	0.06	0.01	0.03	0.00	0.00	0.07	0.00	0.02	0.02

ST11-26	ST11-27	ST11-28	ST11-29	ST11-30	ST11-32	ST11-33	ST11-39	ST11-40	ST11-42	ST11-44	ST11-46
641	653	665	677	688	698	714	756	765	804	839	871
Gab	Ap Mt Cpx	Ap Mt Cpx	Ap Mt Cpx	Gab	Mt Cpx	Mt Cpx	Ore	Ore	Ol Gab	Gab	Ol Gab
MZ	MZ	MZ	MZ	MZ	MZ	MZ	LZ	LZ	LZ	LZ	LZ
II	II	II	II	I	I	I					
3	3	3	3	3	3	3	3	3	3	3	3
67,283	63,816	55,592	66,827	93,146	23,218	17,740	86,201	64,112	33,409	11,681	47,662
26,389	19,779	28,299	22,791	69,061	19,506	15,584	8411	20,121	25,649	12,584	24,165
3145	2342	3654	2665	6638	2294	1380	2954	2098	1757	738	2520
1557	14,828	9530	4494	16,388	3926	3623	5345	5816	5986	882	8082
4.29	5.34	2.89	4.73	4.49	2.50	2.61	6.43	5.54	2.99	1.44	2.52
4095	4216	3593	4416	13,971	3991	4815	4562	4367	4784	5151	4384
253.51	29.40	43.31	58.60	144.37	47.45	37.54	67.41	212.97	950.80	813.30	2360.44
150.85	43.35	67.15	81.35	323.35	143.05	125.71	40.42	131.13	125.75	68.33	136.79
51.23	11.54	2.36	15.53	139.76	49.77	40.65	154.81	532.64	674.51	637.94	448.49
8.37	259.49	3.96	7.51	1.85	0.39	10.86	26.64	5.68	7.18	1.60	-0.52
74.81	64.38	76.13	66.25	253.62	82.79	76.16	47.84	62.48	88.25	59.12	89.70
0.74	81.27	0.11	8.45	0.20	0.38	0.03	26.16	0.09	0.11	6.17	0.15
0.00	7.61	0.00	0.02	0.02	0.02	0.00	0.11	0.01	0.03	0.01	0.00
4.08	2.73	2.31	3.08	6.41	0.48	1.00	3.81	2.19	1.25	0.43	2.02
0.17	0.35	0.38	0.39	0.00	0.00	0.20	0.39	0.04	0.04	0.00	0.12
0.18	0.18	0.08	0.10	0.27	0.04	0.01	0.15	0.09	0.06	0.02	0.08
0.04	0.03	0.04	0.04	0.00	0.03	0.00	0.04	0.05	0.00	0.00	0.01

Table 2 (*continued*)

ST11-08	ST11-09		ST11-13	ST11-15		ST11-18				ST11-42	ST11-46		
363	381		443	471		517				804	871		
Ap Gab	Ap Mt Cpx		Ap Mt Cpx	Ap Mt Cpx		Ap Mt Cpx				Ol Gab	Ol Gab		
MZ	MZ		MZ	MZ		MZ				LZ	LZ		
V	V		IV	IV		IV							
8-Ol-Mt-1	9-Ol-Mt-1	9-Ol-Mt-2	13-Ol-Mt-1	15-Ol-Mt-1	15-Ol-Mt-2	18-Ol-Mt-1	18-Ol-Mt-2	18-Ol-Mt-3	18-Ol-Mt-4	42-Ol-Mt-1	46-Ol-Mt-1	46-Ol-Mt-2	46-Ol-Mt-3
Magnetite inclusions within olivine													
50,158	60,146	60,268	49,707	78,758	48,825	59,719	61,183	58,316	63,540	33,728	37,376	25,058	38,564
23,560	20,893	21,137	20,343	46,163	21,055	19,166	21,948	20,575	24,204	22,656	19,597	12,027	23,002
2843	4227	4227	3291	5056	3039	3527	3813	3603	3714	1841	1784	854	1686
9368	7412	7765	5513	14,416	6955	8735	9723	9260	11,790	8979	8947	5534	11,749
4.65	4.51	4.45	3.72	4.56	5.04	5.37	6.71	4.27	4.32	2.24	3.20	1.27	1.92
3332	3467	3462	3151	2562	3272	3489	3300	3654	3654	4355	4198	5213	4303
59.52	25.62	26.84	16.25	57.24	28.35	25.01	35.99	16.96	39.60	683.52	1913.60	2706.80	2108.00
102.86	65.94	65.21	131.54	151.05	118.06	73.26	96.62	74.24	51.00	172.61	169.60	143.25	85.93
5.70	1.53	0.79	2.90	2.92	5.61	1.46	5.55	2.32	1.20	666.88	559.36	446.22	335.42
−0.43	0.73	0.43	1.32	3.23	2.14	−0.06	2.93	1.34	0.60	5.70	−2.05	−3.89	4.34
64.98	60.21	61.98	69.62	55.44	67.91	57.95	59.54	57.52	61.38	78.21	83.26	80.94	72.60
0.24	0.79	0.32	0.11	42.29	0.02	1.38	2.34	0.24	5.82	0.00	0.21	0.13	1.27
0.00	0.00	0.00	0.00	2.17	0.00	0.00	0.00	0.00	0.00	0.00	0.00	0.00	0.00
2.54	0.12	0.21	1.78	6.04	3.21	1.31	2.20	0.51	3.18	0.68	4.35	1.72	7.69
0.35	0.74	0.70	0.32	0.75	0.04	0.64	0.15	0.21	0.38	0.00	0.35	0.03	0.22
0.11	0.13	0.21	0.16	0.39	0.05	0.85	0.15	0.15	0.14	0.03	0.08	0.05	0.23
0.02	0.04	0.04	0.03	0.08	0.00	0.04	0.07	0.06	0.07	0.02	0.01	0.02	0.00

ilmenite from the Lower Zone is significantly rich in Zr, Hf, Sc, Nb and Ta relative to that of the magnetite (Fig. 6a). However, magnetite from the Middle Zone is lower in Cr, Ni, Ti, Mn, Mg, Nb, Ta, Hf and Zr (Fig. 6b and c), with magnetite of the (apatite) gabbro having the lowest, but highly variable Ti and Mn contents (Fig. 6c). Ilmenite of the Middle Zone rocks has similar Cr, Ni and higher Mg contents compared with that of magnetite (Fig. 6b and c). Especially, ilmenite enclosed in olivine has the highest in Nb, Ta and Sc contents compared to cumulus ilmenite (Fig. 6b and c). Magnetite from the Upper Zone not only has low Cr and Ni, but also has low Mg, Mn and Ti (Fig. 6d). Ilmenite from the Upper Zone is similar in Cr, Ni and Co contents to magnetite, and three samples have high in Nb and Ta contents (Fig. 6d).

The V and Cr contents of magnetite are positively correlated with previously published V and Cr contents of clinopyroxene (She et al., 2014a) (Fig. 7a and b), whereas two trends in the diagrams of V and Cr in ilmenite vs. V and Cr in both clinopyroxene and magnetite are observed (Fig. 7c–f). The V and Cr in ilmenite from Lower Zone are generally positively correlated with that of clinopyroxene and magnetite (Fig. 7d–f), except for the diagram of V in ilmenite vs. V in clinopyroxene (Fig. 7c). The ilmenite from some layers the Middle and Upper Zones have relatively high V and Cr contents, whereas both clinopyroxene and magnetite have relatively constant V and Cr contents (Fig. 7c–f). The Ti in magnetite is positively correlated with Mg, Mn, Sc and Zr (Fig. 8a–d). The magnetite enclosed in olivine also show similar variable trends in these elemental binary plots with cumulus magnetite (Fig. 8a–d). Similarly, the ilmenite and ilmenite inclusions also show positive correlations of Zr with Sc, Nb and Hf, and Ta with Nb (Fig. 9a–d).

6. Discussion

6.1. Multiple replenishments of magma

Open magma chamber processes were important in interpreting the intermittent disappearance of mineral phases and compositional variations of minerals (She et al., 2014a). In general, compositions of minerals that do not follow normal differentiation trends in stratigraphic levels have been used to explain magma replenishment in layered intrusions (e.g. Namur et al., 2010; Song et al., 2013; Pang et al., 2009, 2010). The intermittent disappearance of olivine and plagioclase are observed in the Taihe intrusion (She et al., 2014a). The amounts of Fe–Ti oxides gradually increase upwards in the Lower Zone. In the Middle Zone, the mafic silicates together with abundant Fe–Ti oxides and cumulus apatite form the lower part of the cyclic units, whereas plagioclase content increases upwards. Each cyclic unit represents a sequence from ultramafic to basic composition. The compatible elements Mg, Ti and Mn in magnetite decrease regularly upwards in each cyclic unit (Fig. 5a–c). Similarly, the minor elements, Mg and Sc, in ilmenite behave progressive decreases, upwards in these cyclic units (Fig. 5d and e). The periodic reversals of elements in magnetite and ilmenite are consistent with the variations of silicate compositions (An of plagioclase and Fo of olivine) (Fig. 5f–h) (She et al., 2014a). The cessation of magmatic differentiation and reversals in mineral composition suggest the Taihe intrusion is an open magma chamber in a magma conduit, in which the composition of the magma is periodically modified due to frequent recharges of more primitive magma.

6.2. Crystallization of magnetite and ilmenite

The upward decreases of the Mg, Ti and Mn in magnetite and Mg, Sc in ilmenite (Fig. 5a–e) reflect the decreases of these elements of the residual magma as a result of silicate and oxide fractionation, suggesting that magnetite and ilmenite are cumulus phases. The study by Pang et al. (2008) has demonstrated that Fe–Ti oxide inclusions in the coeval Panzhihua and Hongge intrusions crystallized at the same time to olivine (Fo = 77–81) and became trapped as inclusion in the growing olivine crystals. The entrapment of Fe–Ti oxides in olivine suggested that magnetite and ilmenite crystallized early from a Fe–Ti enriched magma. In the Taihe intrusion, the phenomenon of subhedral to euhedral magnetite and ilmenite enclosed in olivine (Fo = 62–75) or clinopyroxene (Mg# = 72–79) is common (Fig. 3a–d). Furthermore, these magnetite and ilmenite inclusions within olivine are similar in compositional to cumulus magnetite and ilmenite (Fig. 6a–d). These features suggest that the magnetite and ilmenite join the

Table 3
Summary of LA–ICP–MS analyses for compositions of cumulus ilmenite and ilmenite inclusions enclosed in olivine from the Taihe intrusion.

Sample	ST11-58	ST11-56	ST11-52	ST11-51	ST11-48	ST11-02	ST11-03	ST11-05	ST11-06	ST11-08	ST11-09
Depth/m	81	113	169	173	216	246	270	305	323	363	381
Rock	Ap Gab	Ap Gab	Ap Gab	Ap Mt Cpx	Ap Gab	Ap Mt Cpx	Ap Mt Cpx	Mt Cpx	Ap Mt Cpx	Ap Gab	Ap Mt Cpx
Zone	UZ	UZ	UZ	UZ	UZ	MZ	MZ	MZ	MZ	MZ	MZ
Cycle						VI	VI	VI	VI	V	V
Number	3	2	3	3	3	3	3	3	3	3	3
Minor and trace elements (ppm)											
Ti	357,010	361,195	354,993	350,593	360,777	375,037	362,640	370,903	376,287	354,210	356,897
Al	145	300	142	441	170	453	904	132	145	382	479
Mg	281	339	164	393	245	10,232	20,904	707	13,411	15,998	23,227
Mn	16,074	17,590	15,150	16,418	14,037	13,362	17,891	23,301	17,580	10,872	7510
Sc	4.64	23.20	15.46	9.05	13.71	18.81	27.36	9.99	6.20	33.39	36.99
V	820.31	690.06	588.99	514.70	860.63	487.76	354.96	537.91	217.53	476.14	543.50
Cr	72.17	21.61	458.67	30.22	60.78	189.45	33.28	72.93	31.35	49.79	42.31
Co	6.96	13.78	21.99	21.27	24.61	30.92	13.19	29.46	32.88	18.84	30.92
Ni	1.41	3.63	9.11	22.57	7.45	10.97	8.40	35.92	11.05	2.23	8.08
Cu	7.72	1.74	10.39	9.71	10.17	8.46	6.40	3.32	13.20	8.31	3.89
Ga	0.99	0.39	1.18	6.39	2.06	1.65	1.26	0.99	1.01	1.89	2.22
Sr	1.18	0.21	2.21	2.49	0.31	1.16	0.36	0.34	1.32	0.45	0.82
Y	0.03	0.00	0.07	0.72	0.16	0.04	0.08	0.00	0.07	0.10	0.12
Zr	17.53	118.03	59.18	63.84	33.27	73.26	46.00	20.59	29.79	77.40	93.15
Nb	58.32	90.77	25.72	73.30	15.16	57.01	30.22	12.36	44.78	52.96	54.57
Hf	0.89	2.68	0.86	1.26	0.74	0.96	0.82	0.33	0.38	1.68	2.08
Ta	3.29	6.53	1.69	5.00	0.71	4.02	2.79	1.85	2.89	4.74	4.91

ST11-10	ST11-11	ST11-13	ST11-14	ST11-15	ST11-17	ST11-18	ST11-19	ST11-20	ST11-21	ST11-22	ST11-23	ST11-25
400	415	443	459	471	506	517	534	558	575	589	602	629
Ap Gab	Ap Gab	Ap Mt Cpx	Ap Mt Cpx	Ap Mt Cpx	Ap Mt Cpx	Ap Mt Cpx	Ap Gab	Gab	Ap Mt Cpx	Gab	Gab	Gab
MZ	MZ	MZ	MZ	MZ	MZ	MZ	MZ	MZ	MZ	MZ	MZ	MZ
IV	IV	IV	IV	IV	IV	IV	III	III	III	II	II	II
3	3	3	3	3	3	3	3	3	3	3	3	1
356,033	353,757	361,370	359,577	367,190	354,093	362,323	349,590	343,780	360,627	348,823	361,203	376,500
409	85	328	1880	849	308	692	237	46	771	391	375	585
5428	183	19,923	14,528	20,371	10,486	25,898	597	289	4048	12,086	13,941	13,890
9725	11,913	8415	9146	9194	9287	8024	8630	13,435	7409	7138	10,914	8870
19.43	6.54	28.27	34.88	26.53	24.36	33.27	27.94	11.96	33.75	29.61	30.06	36.75
674.33	768.83	421.96	399.73	417.61	505.91	419.91	683.39	1149.87	616.02	643.82	433.65	336.50
37.99	82.93	20.00	25.51	29.10	17.05	28.26	16.44	108.98	33.78	92.61	43.47	28.00
24.98	10.17	30.82	27.17	31.99	27.08	31.59	32.26	10.65	38.97	24.85	23.83	35.25
10.64	7.72	−0.03	7.05	−0.73	0.09	1.92	4.23	10.38	19.37	1.81	10.04	22.25
12.11	7.96	8.13	3.22	9.29	13.58	6.78	9.12	11.65	446.29	9.22	46.65	17.25
2.10	1.50	1.73	1.63	2.29	1.38	1.78	2.11	1.34	1.45	0.86	1.50	1.35
0.73	9.27	0.12	0.73	0.20	0.07	0.19	0.42	0.38	5.46	0.35	0.10	0.20
0.01	2.85	0.10	0.07	0.11	0.04	0.31	0.01	0.04	0.10	0.00	0.00	0.18
62.51	24.29	78.61	80.12	80.61	68.11	86.48	88.71	25.39	99.95	89.25	90.59	118.00
59.09	32.92	48.59	46.98	54.15	43.11	51.65	68.07	61.18	36.25	47.39	23.29	94.00
1.65	0.73	1.79	1.73	1.95	1.23	1.88	1.86	1.27	1.90	1.72	1.39	1.93
5.14	1.84	3.92	3.80	4.57	3.73	4.11	4.53	3.92	2.96	3.27	1.01	2.83

ST11-26	ST11-27	ST11-28	ST11-29	ST11-30	ST11-32	ST11-33	ST11-39	ST11-40	ST11-42	ST11-44	ST11-46
641	653	665	677	688	698	714	756	765	804	839	871
Gab	Ap Mt Cpx	Ap Mt Cpx	Ap Mt Cpx	Gab	Mt Cpx	Mt Cpx	Ore	Ore	Ol Gab	Gab	Ol Cpx
MZ	MZ	MZ	MZ	MZ	MZ	MZ	LZ	LZ	LZ	LZ	LZ
II	II	II	II	I	I	I					
3	3	3	3	3	3	3	3	3	3	3	3
364,290	367,977	349,020	364,370	366,773	360,880	353,140	366,230	370,763	361,397	367,510	362,527
388	834	564	454	1695	1037	472	1207	299	200	181	293
3755	31,547	16,875	11,533	13,762	6910	9378	6560	5035	8972	320	15,345
9450	6668	7842	7588	9115	11,926	7045	8291	7990	10,870	14,435	7564
22.59	27.08	26.28	28.99	16.52	13.10	25.33	26.41	27.63	22.81	16.19	25.48
511.79	409.85	455.13	449.69	526.46	315.77	689.53	415.19	387.40	475.16	579.30	633.88
42.95	74.36	1.08	39.00	49.10	22.43	30.88	45.39	56.97	165.13	201.20	172.29
35.14	23.85	21.62	25.88	31.26	53.68	45.35	20.50	35.59	36.37	35.72	34.84
8.80	12.76	2.93	13.02	6.64	13.69	15.84	38.11	55.81	34.64	33.78	35.10
6.12	45.28	6.12	12.48	10.58	10.17	14.87	69.71	27.82	11.28	7.82	6.85
1.30	2.02	1.03	1.43	2.93	2.22	2.30	2.06	1.27	1.63	1.40	1.66
0.54	0.52	0.10	0.20	0.36	0.15	0.18	0.14	0.04	1.24	0.18	0.07
0.02	0.10	0.07	0.02	0.02	0.00	0.04	0.04	0.04	0.06	0.00	0.06
134.73	68.73	83.61	94.88	79.73	42.82	79.80	49.07	57.69	54.65	33.95	92.39
56.51	45.10	73.26	48.66	72.74	12.93	53.41	29.01	15.93	43.08	33.33	84.50
2.43	1.49	1.72	1.62	1.88	1.18	1.23	1.03	1.03	1.04	0.69	1.56
4.48	3.38	6.28	3.51	4.53	0.90	3.71	2.21	1.02	2.86	1.96	5.93

Table 3 (*continued*)

ST11-08			ST11-09		ST11-18	ST11-28			ST11-42	ST11-46
363			381		517	665			804	871
Ap Gab			Ap Mt Cpx		Ap Mt Cpx	Ap Mt Cpx			Ol Gab	Ol Cpx
MZ			MZ		MZ	MZ			LZ	LZ
V			V		IV	II				
8-Ol-Ilm-1	8-Ol-Ilm-2	8-Ol-Ilm-3	9-Ol-Ilm-1	9-Ol-Ilm-2	18-Ol-Ilm-1	28-Ol-Ilm-1	28-Ol-Ilm-2	28-Ol-Ilm-3	42-Ol-Ilm-1	46-Ol-Ilm-1
Ilmenite inclusions within olivine										
350,280	351,120	351,480	354,780	357,480	360,880	362,250	357,500	352,300	353,750	295,120
378	364	335	426	410	420	399	678	539	788	5066
14,347	14,834	10,945	15,101	18,255	18,765	13,525	15,552	12,992	11,372	13,301
10,064	8199	8968	9486	7386	9954	8701	7544	9015	10,272	9929
52.36	29.96	37.70	38.74	38.00	40.25	25.74	24.03	23.49	22.62	19.28
827.96	595.84	568.69	719.16	737.50	586.50	464.36	579.69	515.43	252.98	1101.60
13.44	40.32	31.61	182.00	33.25	28.00	2.86	15.39	45.90	153.40	914.60
35.84	30.52	21.98	40.82	22.00	19.50	24.18	20.52	32.40	63.18	114.92
−2.80	−0.56	−1.45	1.56	0.75	−0.75	0.00	6.21	−1.35	52.78	247.18
7.56	7.00	2.90	9.88	2.25	0.75	10.40	8.64	11.88	14.56	107.44
1.29	0.92	0.90	2.29	1.00	1.43	1.98	1.40	1.62	2.65	27.88
0.06	0.27	0.37	0.44	0.08	0.25	0.05	0.10	0.30	0.15	0.63
0.10	0.06	0.00	0.22	0.16	0.04	0.10	0.14	0.02	0.00	0.00
108.64	77.56	80.91	124.28	118.25	93.75	113.36	85.86	110.43	26.52	118.66
70.56	60.76	61.48	71.50	76.75	51.75	89.70	76.68	82.62	9.91	36.75
1.68	1.62	1.89	2.26	2.00	2.05	2.55	1.70	2.89	0.62	2.28
5.96	6.61	6.84	6.34	7.25	4.33	7.67	6.37	7.05	0.77	3.16

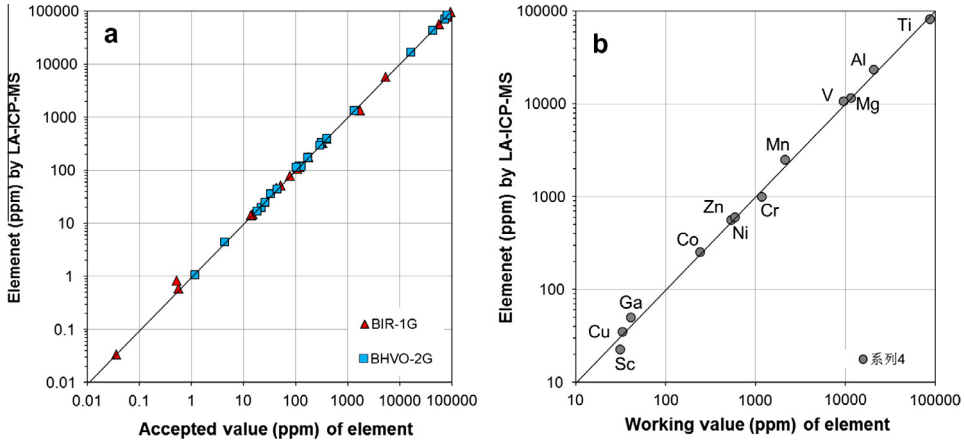

Fig. 4. LA-ICP-MS analyses of international reference materials (a) and BC-28 magnetite from the Bushveld Complex (b). BC-28 magnetite data are from the Dare et al. (2014).

liquidus at early stage of evolution of magma in the Taihe magma chamber.

The concentration of an element in magnetite and ilmenite depends on the concentration of the element in the parental magma from which they crystallize, and whether other minerals are competing for that element, and the partition coefficient of the element between mineral and magma (Dare et al., 2014; Nadoll et al., 2014; Charlier et al., 2007). Therefore, the behavior of trace elements during fractionation of magma can be recorded by crystallization of magnetite and ilmenite. For example, the content of elements compatible during fractionation (e.g. Cr, Ni, Mg) are highest in early forming oxides and decrease with stratigraphic height, whereas most other elements are incompatible and increase in oxides (Dare et al., 2014). The compatible elements Cr and Ni are concentrated in the magnetite and ilmenite from the Taihe Lower Zone (Fig. 6a) suggesting that these Fe–Ti oxides crystallize from a relatively primitive magma. In contrast, both magnetite and ilmenite from the Middle Zone have low in Cr and Ni contents (Fig. 6b and c), indicating their parental magmas are more evolved than that of the Lower Zone. Most of magnetite of the (apatite)-magnetite clinopyroxenite in the lower part shows higher in Ti, Mg and Mn than that of the (apatite) gabbro in the upper part of the Middle Zone (Fig. 6b and c). This can be ascribed to be the result of the Fe–Ti oxides and mafic silicates saturate and accumulate on the lower parts of cyclic units, and then the residual magma formed overlying (olivine) gabbro. This is consistent with the ilmenite from the (apatite) gabbro having low Mg concentrations relative to that of (apatite)-magnetite clinopyroxenite (Fig. 6b and c). The Taihe Upper Zone rocks have lowest Cr, Ni, Mg, Ti in magnetite, and low in Cr, Ni, Mg and high in Zr, Hf, Nb, Ta in ilmenite (Fig. 6d) suggesting that the magnetite and ilmenite crystallize from more evolved residual magma.

The concentration of the element in magnetite or ilmenite is also controlled by whether other minerals crystallizing at the same time are competing for the element. Once large amounts of ilmenite become liquidus mineral, the Ti content in magma will sharply decrease in the Taihe intrusion (She et al., 2014a,b). Relatively high Ti content in magnetite of the Lower Zone rocks (Fig. 6a) indicates crystallization of ilmenite has insignificant effect on the Ti partitioning of magnetite. Sc is weakly compatible to magnetite and clinopyroxene (Dare et al., 2012; Hauri et al., 1994). However, Nb, Ta and Sc are preferentially partitioned into ilmenite

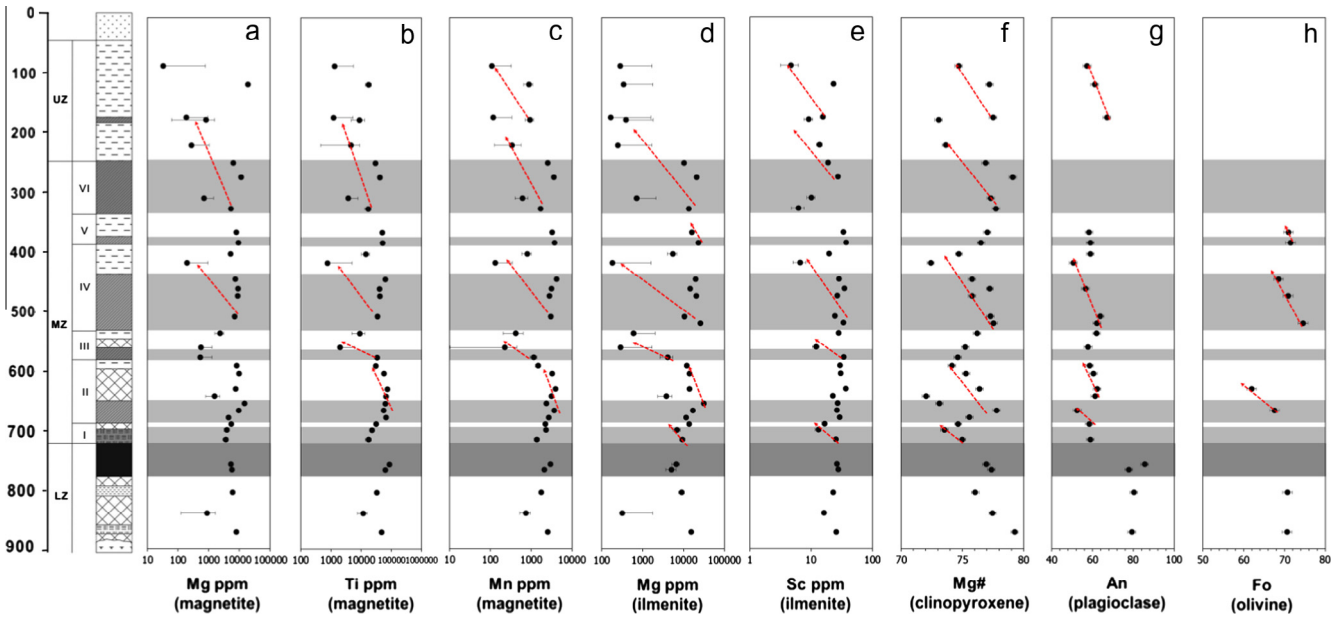

Fig. 5. Chemostratigraphic variation in compositions of oxide and silicate minerals of the Taihe intrusion. Clinopyroxene, plagioclase and olivine data are from She et al. (2014a).

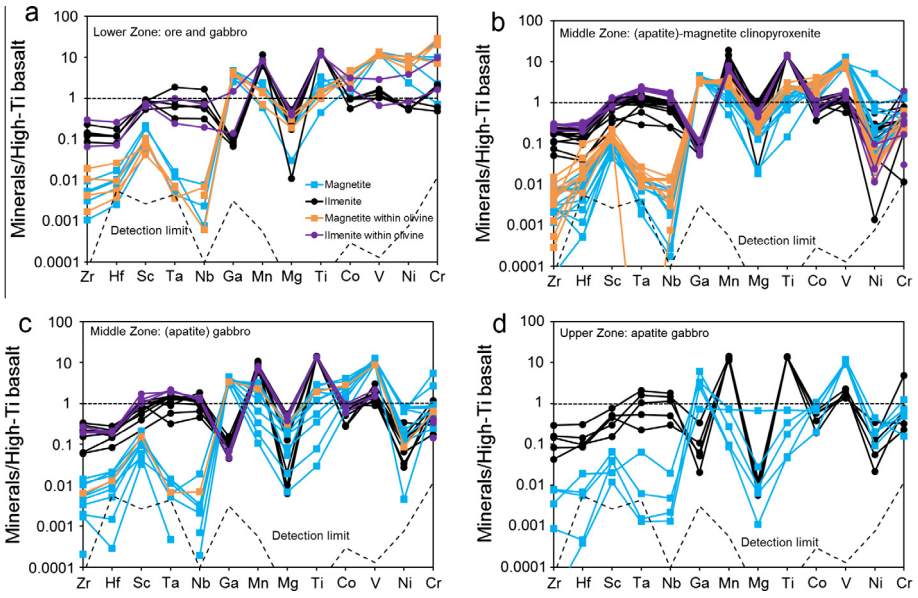

Fig. 6. Normalized multielement variation diagrams for magnetite and ilmenite of the Taihe intrusion. Normalized to Emeishan high-Ti basalt using average values from Xiao et al. (2004), Qi and Zhou (2008) and Song et al. (2008). The order of trace elements from lefe to right is with increasing compatibility into magnetite (after Dare et al., 2014).

(Klemme et al., 2006). In Fig. 6a, high Sc, Nb, Ta contents in ilmenite from the Lower Zone suggest crystallization of magnetite and clinopyroxene barely has any significant effect on Sc, Nb and Ta partitioning of ilmenite. The magnetite from the Lower Zone has high in Cr and Ni contents (Fig. 6a), suggesting the magnetite may crystallize earlier than or simultaneously with ilmenite, olivine and clinopyroxene because Cr and Ni are also compatible to these minerals (Dunn and Sen, 1994; Hauri et al., 1994; Klemme et al., 2006). This is consistent with some magnetite inclusions enclosed in olivine or clinopyroxene crystals (Fig. 3a and b). The V and Cr in magnetite are positively correlated with V and Cr in clinopyroxene (Fig. 7a and b), demonstrating both magnetite and clinopyroxene crystallize almost simultaneously. The clinopyroxene from the Lower Zone contains relatively high in V (Fig. 7c), indicating that it crystallizes early. Positive correlation of Cr in clinopyroxene with Cr in ilmenite from the Lower Zone demonstrates the timing of saturation of clinopyroxene is close to that of ilmenite (Fig. 7d). Moreover, positive correlations between ilmenite and magnetite for Cr and Ni from the Lower Zone (Fig. 7e and f) also indicate that magnetite and ilmenite saturate at the same time. These features suggest that magnetite, ilmenite and clinopyroxene are main cumulus phases in early stage of fractionation of the Lower Zone parental magma.

In the Middle Zone, similar Cr and Ni contents in most of magnetite and ilmenite (Fig. 6b and c) may indicate that magnetite crystallizes later than or simultaneously with ilmenite because

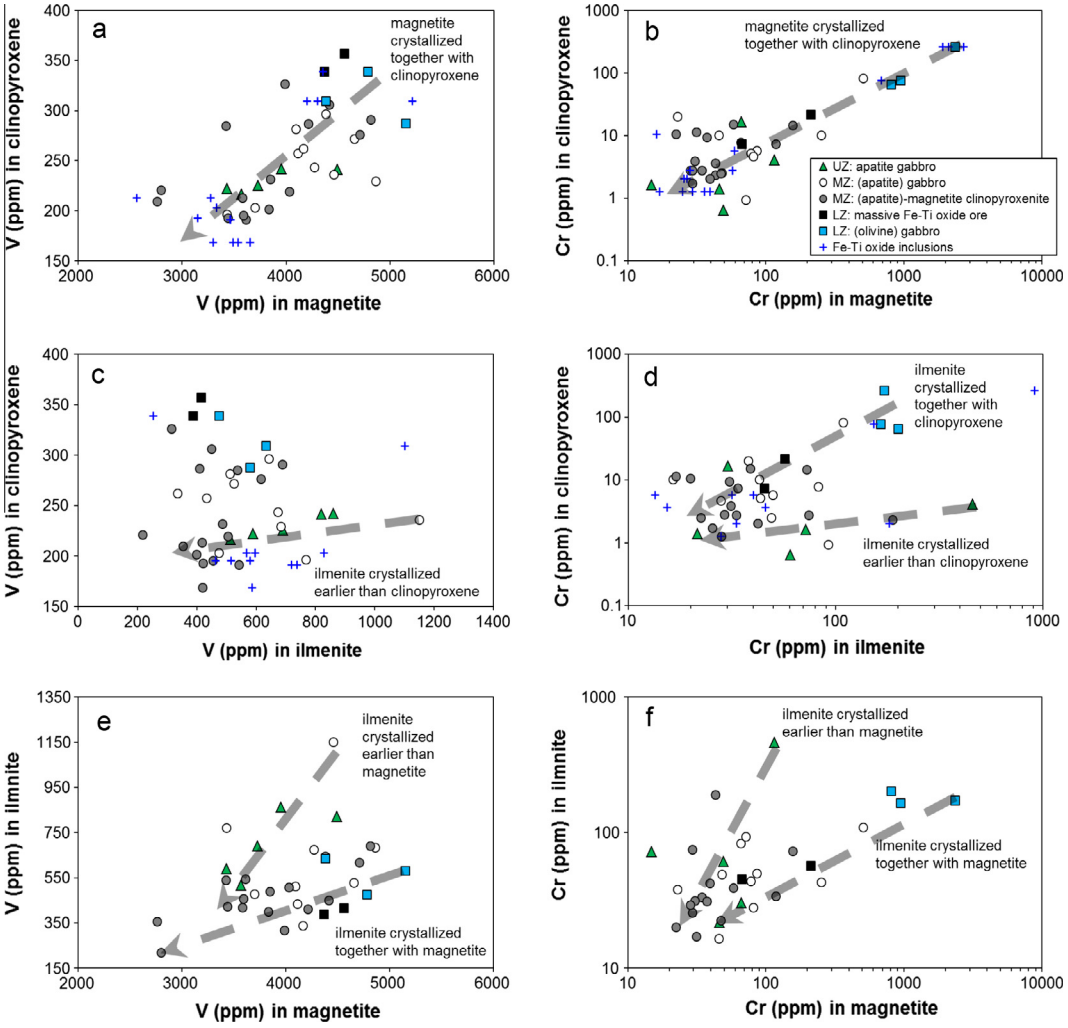

Fig. 7. Binary plots of V in clinopyroxene vs. V in magnetite (a), Cr in clinopyroxene vs. Cr in magnetite (b), V in clinopyroxene vs. V in ilmenite (c), Cr in clinopyroxene vs. Cr in ilmenite (d), V in ilmenite vs. V in magnetite (e), Cr in ilmenite vs. Cr in magnetite (f) for different rock types of the Taihe intrusion. The clinopyroxene data are from the She et al. (2014a).

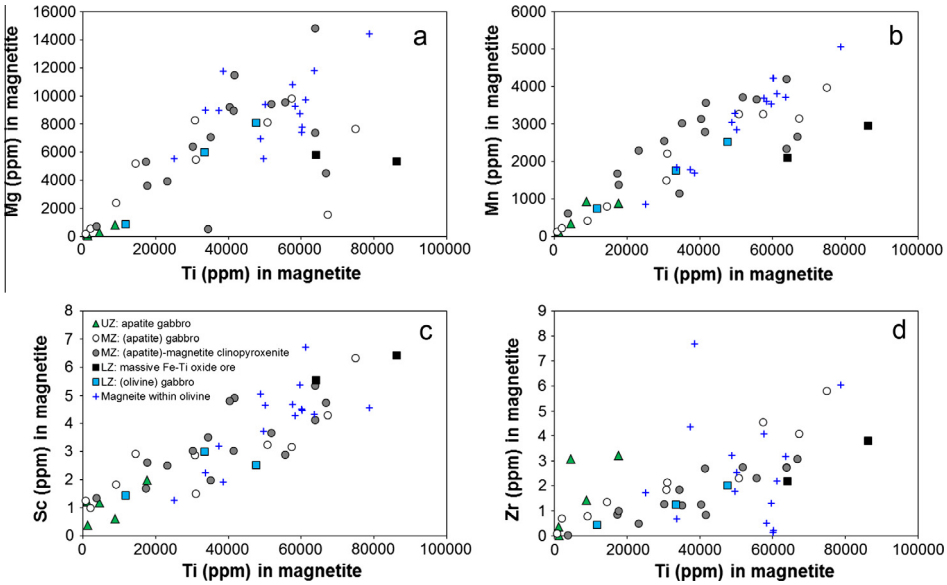

Fig. 8. Binary plots of Ti vs. Mg (a), Mn (b), Sc (c) and Zr (d) in magnetite for different rock types of the Taihe intrusion.

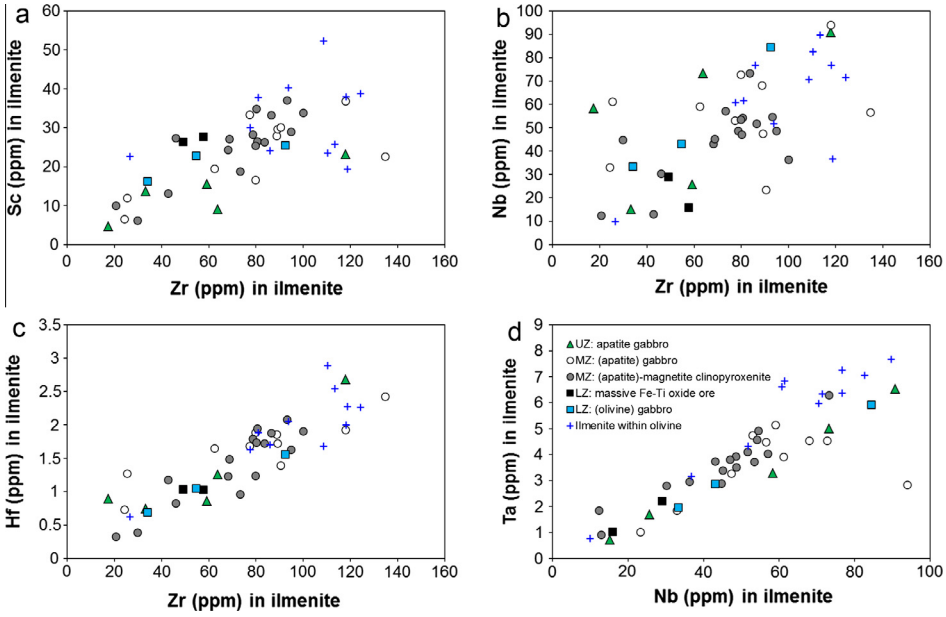

Fig. 9. Binary plots of Zr vs. Sc (a), Hf (b) and Nb (c), and Nb vs. Ta (d) in ilmenite for different rock types of the Taihe intrusion.

magnetite has higher partition coefficients for Cr and Ni than that of ilmenite (Dare et al., 2012). Moreover, low Mg contents in magnetite also suggest that the crystallizing olivine, clinopyroxene and ilmenite are competing with magnetite for the element (Fig. 6b and c). The magnetite of (apatite) gabbro of the Middle Zone shows highly variable Ti and Mn contents (Fig. 6c), suggesting that crystallization of ilmenite has significant effect on Ti and Mn partitioning into magnetite. High Nb, Ta and Sc in ilmenite (in particular ilmenite inclusions within olivine) and extremely low Nb and Ta in magnetite (Fig. 6b and c), suggest that abundant ilmenite crystallization resulted in depletion of these elements in the magma. In the Upper Zone rocks, Cr, Ni, Co, Ti, Mg and Mn in magnetite are significant by lower than that of the Lower Zone (Fig. 6d). This is due to crystallization of ilmenite and clinopyroxene which can decease dramatically the concentrations of these elements in magma, and suggests that magnetite crystallize later than or simultaneously with ilmenite. It is noteworthy that the ilmenite from some levels of the Middle and Upper Zones has highly variable V and Cr contents, whereas the clinopyroxene and magnetite have low in V and Cr contents (Fig. 7c–f), implying that the ilmenite crystallized slightly earlier than clinopyroxene and magnetite in these stratigraphic levels.

6.3. Factors controlling the early saturation of Fe–Ti oxides

The early crystallization of magnetite and ilmenite in the Taihe intrusion can be resulted from three factors: (1) composition of parental magma; (2) oxygen fugacity (fO_2); (3) the presence of volatiles in the magma.

The study of melt inclusions within the olivine phenocrysts of the Emeishan high-Ti picrite suggested that the primary magma of the Fe–Ti oxide ore-bearing layered intrusions in central ELIP was already rich in Fe and Ti (~12 wt% FeOt, ~3 wt% TiO_2) and that it originated from mantle source (Kamenetsky et al., 2012). The high-Ti picritic magma became more enriched in Fe and Ti (~16.7 wt% FeOt, ~4.9 wt% TiO_2) as a result of fractionation of silicates to deep-seated magma chambers (Song et al., 2013). The Taihe Lower Zone rocks have the relatively low Fo_{71} content of olivine and abundant oxide-exsolution lamellae in clinopyroxene, indicating that the Lower Zone parental magma was an evolved Fe–Ti-rich magma (She et al., 2014a). This is consistent with high Ti and V concentrations in magnetite from the Lower Zone (Fig. 6a). When such Fe–Ti-rich magma intruded into the Taihe magma chamber from deeper levels, magnetite and ilmenite became the early liquidus mineral and formed the Fe–Ti oxide ore layers of the Lower Zone. However, magnetite from the Middle Zone not only contains high Ti and V, but also has low content of compatible elements Cr and Ni (Fig. 6b and c). The ilmenite inclusions enclosed by olivine from the Middle Zone have higher Nb and Ta than that of the Lower Zone (Fig. 6b and c). These features suggest that the parental magmas that formed the Middle Zone were more evolved and riched in incompatible elements lower in compatible elements (Cr, Ni). Previous study showed the Taihe Middle and Upper Zones rocks have higher ilmenite/magnetite ratios (0.5–2) than that of Lower Zone (She et al., 2014a). Additionally, as discussed above, ilmenite from some stratigraphic levels of the Middle and Upper Zones crystallized slightly earlier than clinopyroxene and magnetite. As the crystallization of ilmenite is mainly controlled by the TiO_2 content in magma (Charlier et al., 2006; Klemme et al., 2006), high ilmenite/magnetite ratios and early crystallization of ilmenite demonstrate that the parental magmas of the Middle and Upper Zones had higher TiO_2 contents than that of the Lower Zone. She et al. (2014a,b) reported that the plagioclase has relatively high An (78–86) and the clinopyroxene contains 65–263 ppm Cr and 66–83 ppm Ni in the Taihe Lower Zone rocks. Whereas in the Middle Zone, the clinopyroxene has remarkable low concentrations of Cr (<20 ppm) and Ni (<10 ppm) and plagioclase is low in An51–67. This indicates that the Fe–Ti–P enriched parental magma of the Middle Zone represents a more evolved melt than that of Lower Zone. They speculated that such Fe–Ti–P enriched magma was produced by mixing between a Fe–Ti enriched magma from deep level and a P_2O_5 saturated resident magma as well as remelting of fusible minerals such as apatite and ilmenite in a middle-level magma chamber. Therefore, it can be inferred that the high TiO_2 contents in the parental magma of the Middle and Upper Zones may have resulted from the remelting of pre-existing ilmenite in the middle-level magma chamber.

Melting experiments in ferrobasalts demonstrate that the partitioning of V in magnetite is a function of oxygen fugacity (Toplis and Corgne, 2002 and references therein). Oxygen fugacity determines the $V^{3+}/V^{4+}/V^{5+}$ ratios in magma, and the magnetite-melt partition coefficient for V^{3+} is much higher than that to V^{4+} and

V^{5+} (Toplis and Corgne, 2002). In other words, magnetite that crystallized under reducing conditions is richer in V than crystallization of magnetite under oxidizing condition due to high V^{3+} content in magma. The V contents of magnetite (2562–5213 ppm, Table 1) from the Taihe intrusion are much lower than that of the Bushveld Complex (~13,000 ppm V in magnetite, FMQ to FMQ + 1, Cawthorn and Molyneux, 1986) and the Fedorivka layered intrusion (~18,500 ppm V, FMQ-1.4 to FMQ + 0.7, Duchesne et al., 2006), and are similar to that of Suwalki anorthosite (2000–6700 ppm V, FMQ + 2 to FMQ + 3.5, Charlier et al., 2009). The relatively low V contents in magnetite from the Taihe intrusion indicate that it crystallized under higher oxygen fugacity (Shellnutt et al., 2011). The experiment of Toplis and Carroll (1995) showed that magnetite crystallized earlier than ilmenite in oxidizing conditions, whereas ilmenite crystallized before magnetite at relatively lower oxygen fugacity. In the Taihe intrusion, the petrography and compositions of Fe–Ti oxides indicate that the ilmenite crystallizes earlier than or simultaneously with magnetite and clinopyroxene. Therefore, oxygen fugacity only affects the stability field of magnetite and ilmenite in a relatively low FeOt and TiO_2 parental magma.

The experimental studies by Sisson and Grove (1993) and Botcharnikov et al. (2008) demonstrated that the addition of high H_2O contents to basaltic magma tends to lower the crystallization temperature of plagioclase but has a lesser effect on Fe–Ti oxides. Thus, addition of H_2O may cause magnetite and ilmenite to appear earlier than plagioclase in magma. Howarth et al. (2013) suggested the parental magma of the Panzhihua intrusion was H_2O-rich and Fe–Ti oxide crystal-rich magmas, and high H_2O content triggered the early crystallization of oxides. However, only small amounts of hydrous minerals such as hornblende are present at most of stratigraphic levels in the Taihe intrusion, suggesting that H_2O is not directly related to early appearance of Fe–Ti oxides (Shellnutt et al., 2011). Therefore, it can be concluded that early crystallization of ilmenite and magnetite in the Taihe intrusion is neither the result from high oxygen fugacity nor high H_2O content in magma. The high FeO_t and TiO_2 contents of the Lower Zone parental magma are the most reasonable explanation for the early crystallization of magnetite and ilmenite.

6.4. Origin of the Taihe Fe–Ti–V oxide deposit

The origin of Fe–Ti–V oxide ore deposits hosted in the layered intrusions of the central ELIP is highly debated. Some workers propose that the Fe–Ti oxide ores in the Panzhihua, Hongge and Baima intrusions are the result of solidification of an immiscible Fe-rich liquid (Zhou et al., 2005; Wang and Zhou, 2013; Liu et al., 2014a,b). However, a number of experiments indicate that phosphorus is essential for formation of such immiscible Fe-rich liquid during magma differentiation (Philpotts, 1967; Watson, 1976; Visser and van Groos, 1979; Bogaerts and Schmidt, 2006; Charlier and Grove, 2012). Due to absence of cumulus apatite in the Fe–Ti oxide ores of the Panzhihua, Baima and Hongge deposits, it implies that phosphorus does not play a direct role in oxide ore formation. Therefore, another workers called upon fractional crystallization and gravitational accumulation of Fe–Ti oxide to explain the formation of these Fe–Ti oxide ore deposits (Pang et al., 2008, 2009; Ganino et al., 2008; Song et al., 2013; Howarth et al., 2013; Zhang et al., 2012; Bai et al., 2012; Luan et al., 2014; Shellnutt et al., 2009, 2011, 2014; Shellnutt and Jahn, 2010). They concluded that stratiform Fe–Ti oxide layers resulted from gravitational sorting and settling of Fe–Ti oxides from the following evidence: (1) early saturation of Fe–Ti oxides, (2) the presence of abundant Fe–Ti oxide inclusions within olivine, (3) frequent replenishments of the Fe–Ti enriched magmas, (4) and the important oxide ores occur in the lower or middle parts of the intrusions.

Different from the other coeval Fe–Ti oxide ore-bearing intrusions, the Taihe intrusion not only contains massive oxide ores in the Lower Zone but also has apatite-rich disseminated ores in the Middle Zone (Fig. 2). In the Taihe Lower Zone, at the time of Fe–Ti oxide crystallization, the parental magma of the Lower Zone was able to crystallize relatively primitive plagioclase (An = 78–86) and olivine (Fo = 71) (She et al., 2014a), suggesting that the Fe–Ti oxide appears at relatively high temperature. The Cr and V contents of magnetite from the Lower Zone are positively correlated with Cr and V contents of clinopyroxene (Fig. 7a and b), also suggesting that magnetite crystallized together with clinopyroxene at an early stage of magma differentiation. Moreover, Fe–Ti oxide inclusions enclosed in olivine of the Lower Zone are similar in compositional to those of the cumulus oxides (Fig. 6a). Therefore, the occurrence of Fe–Ti oxide ores in the Lower Zone is best explained by early crystallization and gravitational accumulation of Fe–Ti oxide crystals.

However, abundant cumulus apatite occurs in the Taihe Middle Zone (Fig. 3c and d), indicating that phosphorus may play a direct role in formation of thick apatite-rich disseminated ores at the base of each cyclic unit. Liquid–liquid immiscibility propose that silicate minerals such as olivine, clinopyroxene and plagioclase crystallized from the Si-rich liquid, whereas Fe–Ti oxides and apatite crystallized from the Fe-rich melts which segregated from the co-genetic Si-rich liquid (Philpotts, 1967; Kolker, 1982; Jakobsen et al., 2005; VanTongeren and Mathez, 2012; Chen et al., 2013). Although some experimental studies by Tollari et al. (2008) and Lester et al. (2013) showed that minor silicate minerals may crystallize from the conjugate immiscible Fe-rich liquids, apatite and Fe–Ti oxides are still main crystallized phases during decrease of liquid temperature. In contrast, the apatite–magnetite clinopyroxenites of the Taihe Middle Zone contain 20–50% Fe–Ti oxides, 6–12% apatite, and as high as 50–70% clinopyroxene and olivine, indicating that they cannot crystallize from the immiscible Fe-rich liquids. A number of experimental studies demonstrated that immiscible Fe-rich melts not only are rich in Fe, P and Ti, but also contain high concentrations of trace element Sr, Th, U, REE, Zr, Hf, Nb and Ta (Veksler et al., 2006, 2007; Lester et al., 2013; Shearer et al., 2001; Charlier and Grove, 2012). If magnetite and ilmenite crystallized from such immiscible Fe-rich melts, they would highly rich in trace element Zr, Hf, Nb and Ta. However, as shown in Fig. 6a–d, magnetite of the Taihe intrusion is highly depleted in Zr, Hf, Nb and Ta. Although ilmenite has higher partition coefficients for Zr, Hf, Nb and Ta than that of magnetite (Klemme et al., 2006), the ilmenite of the Taihe intrusion shows slightly higher Nb, Ta, and much lower Zr, Hf contents than coeval high-Ti basalts (Fig. 6a–d). These trace element features in magnetite and ilmenite of the Taihe intrusion are difficult to be interpreted to crystallize from an immiscible Fe-rich melts. In reality, magnetite and ilmenite most probably crystallized from the Fe–Ti–(P)-rich basaltic magma. Furthermore, the Ti contents of magnetite from the Taihe rocks and ores are positively correlated with Mg, Mn, Sc and Zr (Fig. 8a–d), suggesting these elements fractionated continuously during differentiation of magma. The lack of a compositional gap in magnetite from the oxide ores and host rocks strongly suggests that magnetite crystallized from homogeneous silicate magma rather than immiscible Fe-rich melts. This conclusion is also supported by positive correlations of Zr with Sc, Nb and Hf, and Nb with Ta in ilmenite throughout the Taihe intrusion (Fig. 9a–d). Although abundant apatite is present at the disseminated ores of the Middle Zone, phosphorus may play a role in stabilizing Fe^{3+} in magma and promote iron enrichment in the magma through suppression of magnetite crystallization (Toplis et al., 1994; Tollari et al., 2006). Once abundant magnetite crystallizes from Fe–Ti–P-rich magma, high phosphorus content and decline of Fe^{3+} in magma would trigger saturation in apatite (Toplis

et al., 1994; Tollari et al., 2006). Therefore, the early crystallization and gravitational accumulation of Fe–Ti oxide and apatite along with mafic silicates from the Fe–Ti–P-rich parental magma are the most convincing explanation for formation of apatite–magnetite clinopyroxenite in the Taihe Middle Zone.

7. Conclusions

This study provides petrographic and geochemical evidence for early crystallization of magnetite and ilmenite of the Taihe intrusion. Ilmenite saturated earlier than magnetite and clinopyroxene in some stratigraphic levels of the Middle Zone. The sequence of crystallization and compositions of magnetite and ilmenite indicate that neither high oxygen fugacity nor high water content resulted in the early saturation of Fe–Ti oxides. Saturation of magnetite and ilmenite was controlled mainly by high Fe and Ti concentrations of the parental magmas. Relatively low Nb, Ta, Zr, Hf contents of magnetite and ilmenite suggest they did not crystallize from an immiscible Fe-rich liquid. The continual variations in trace element contents of the magnetite and ilmenite indicate that they most likely formed from an oxide-saturated Fe–Ti–(P)-rich basaltic magma. Early crystallization and gravitational accumulation of magnetite and ilmenite along with mafic silicates are the most reasonable explanation for formation of the Fe–Ti oxide ores of the Taihe intrusion.

Acknowledgments

We thank Mr. Ting Zhou and Mrs. Zi-Hui Dai for the LA–ICP–MS analysis. Mr. Yu Wei is appreciated for field assistance. We are very grateful to the editors, Dr. Sarah Dare and Dr. Greg Shellnutt for comments on a preliminary version of our manuscript. This study was funded by the National Basic Research Program of China (2012CB416804), research grants from State Key Laboratory of Ore Deposit Geochemistry (SKLOG-ZY125-06) and CAS/SAFEA International Partnership Program for Creative Research Teams (KZZD-EW-TZ-20) and NSFC (40730420) to Xie-Yan Song.

References

Ali, J.R., Thompson, G.M., Zhou, M.F., Song, X.Y., 2005. Emeishan large igneous province, SW China. Lithos 79, 475–489.

Bai, Z.J., Zhong, H., Naldrett, A.J., Zhu, W.G., Xu, G.W., 2012. Whole-Rock and Mineral Composition Constraints on the Genesis of the Giant Hongge Fe–Ti–V Oxide Deposit in the Emeishan Large Igneous Province, Southwest China. Econ. Geol. 107, 507–524.

Bogaerts, M., Schmidt, M., 2006. Experiments on silicate melt immiscibility in the system Fe_2SiO_4–$KAlSi_3O_8$–SiO_2–CaO–MgO–TiO_2–P_2O_5 and implications for natural magmas. Contrib. Miner. Petrol. 152, 257–274.

Botcharnikov, R., Almeev, R., Koepke, J., Holtz, F., 2008. Phase relations and liquid lines of descent in hydrous ferrobasalt-implications for the Skaergaard intrusion and Columbia River flood basalts. J. Petrol. 49, 1687–1727.

Cawthorn, R.G., Molyneux, T.G., 1986. Vanadiferous magnetite deposits of the Bushveld Complex. In: Anhaeusset, C.R., Maske, S. (Eds.), Mineral Deposits of Southern Africa. Geol. Soc. South Africa, Johannesburg, pp. 1251–1266.

Charlier, B., Duchesne, J.C., Vander Auwera, J., 2006. Magma chamber processes in the Tellnes ilmenite deposit (Rogaland Anorthosite Province, SW Norway) and the formation of Fe–Ti ores in massif-type anorthosites. Chem. Geol. 234, 264–290.

Charlier, B., Grove, T.L., 2012. Experiments on liquid immiscibility along tholeiitic liquid lines of descent. Contrib. Miner. Petrol. 164, 27–44.

Charlier, B., Namur, O., Duchesne, J.-C., Wiszniewska, J., Parecki, A., Vander Auwera, J., 2009. Cumulate origin and polybaric crystallization of Fe–Ti oxide ores in the suwalki anorthosite, northeastern Poland. Econ. Geol. 104, 205–221.

Charlier, B., Skår, Ø., Korneliussen, A., Duchesne, J.-C., Vander Auwera, J., 2007. Ilmenite composition in the Tellnes Fe–Ti deposit, SW Norway: fractional crystallization, postcumulus evolution and ilmenite–zircon relation. Contrib. Miner. Petrol. 154, 119–134.

Chen, W.T., Zhou, M.-F., Zhao, T.-P., 2013. Differentiation of nelsonitic magmas in the formation of the ~1.74 Ga Damiao Fe–Ti–P ore deposit, North China. Contrib. Miner. Petrol. 165, 1341–1362.

Chung, S.L., Jahn, B., 1995. Plume-lithosphere interaction in generation of the Emeishan flood basalts at the Permian–Triassic boundary. Geology 23, 889–892.

Dare, S.A.S., Barnes, S.-J., Beaudoin, G., 2012. Variation in trace element content of magnetite crystallized from a fractionating sulfide liquid, Sudbury, Canada: implications for provenance discrimination. Geochim. Cosmochim. Acta 88, 27–50.

Dare, S.A.S., Barnes, S.-J., Beaudoin, G., Méric, J., Boutroy, E., Potvin-Doucet, C., 2014. Trace elements in magnetite as petrogenetic indicators. Miner. Deposita 49, 785–796.

Duchesne, J.-C., Shumlyanskyy, L., Charlier, B., 2006. The Fedorivka layered intrusion (Korosten Pluton, Ukraine): an example of highly differentiated ferrobasaltic evolution. Lithos 89, 353–376.

Dunn, T., Sen, C., 1994. Mineral/matrix partition coefficients for orthopyroxene, plagioclase, and olivine in basaltic to andesitic systems: a combined analytical and experimental study. Geochim. Cosmochim. Acta 58, 717–733.

Dupuis, C., Beaudoin, G., 2011. Discriminant diagrams for iron oxide trace element fingerprinting of mineral deposit types. Miner. Deposita 46, 319–335.

Ganino, C., Arndt, N.T., Zhou, M.F., Gaillard, F., Chauvel, C., 2008. Interaction of magma with sedimentary wall rock and magnetite ore genesis in the Panzhihua mafic intrusion, SW China. Miner. Deposita 43, 677–694.

Hauri, E.H., Wagner, T.P., Grove, T.L., 1994. Experimental and natural partitioning of Th, U, Pb and other trace elements between garnet, clinopyroxene and basaltic melts. Chem. Geol. 117, 149–166.

Hou, T., Zhang, Z.-C., Encarnacion, J., Santosh, M., 2012. Petrogenesis and metallogenesis of the Taihe gabbroic intrusion associated with Fe–Ti–oxide ores in the Panxi district, Emeishan Large Igneous Province, southwest China. Ore Geol. Rev. 49, 109–127.

Howarth, G.H., Prevec, S.A., Zhou, M.-F., 2013. Timing of Ti-magnetite crystallisation and silicate disequilibrium in the Panzhihua mafic layered intrusion: implications for ore-forming processes. Lithos 170–171, 73–89.

Huang, X.-W., Zhou, M.-F., Qi, L., Gao, J.-F., Wang, Y.-W., 2013. Re–Os isotopic ages of pyrite and chemical composition of magnetite from the Cihai magmatic–hydrothermal Fe deposit, NW China. Miner. Deposita 48, 925–946.

Jakobsen, J.K., Veksler, I.V., Tegner, C., Brooks, C.K., 2005. Immiscible iron- and silica-rich melts in basalt petrogenesis documented in the Skaergaard intrusion. Geology 33, 885–888.

Jang, Y.D., Naslund, H.R., 2003. Major and trace element variation in ilmenite in the Skaergaard intrusion: petrologic implications. Chem. Geol. 193, 109–125.

Kamenetsky, V.S., Chung, S.L., Kamenetsky, M.B., Kuzmin, D.V., 2012. Picrites from the Emeishan Large Igneous Province, SW China: a compositional continuum in primitive magmas and their respective mantle sources. J. Petrol. 53, 2095–2113.

Klemme, S., Günther, D., Hametner, K., Prowatke, S., Zack, T., 2006. The partitioning of trace elements between ilmenite, ulvospinel, armalcolite and silicate melts with implications for the early differentiation of the moon. Chem. Geol. 234, 251–263.

Kolker, A., 1982. Mineralogy and geochemistry of Fe–Ti oxide and apatite (nelsonite) deposits and evaluation of the liquid immiscibility hypothesis. Econ. Geol. 77, 1146–1158.

Lester, G., Kyser, T., Clark, A., Layton-Mathews, D., 2013. Trace element partitioning between immiscible silicate melts with H_2O, P, S, F, and Cl. Chem. Geol. 357, 178–185.

Liu, P.-P., Zhou, M.-F., Chen, W.T., Boone, M., Cnudde, V., 2014a. Using Multiphase Solid Inclusions to Constrain the Origin of the Baima Fe–Ti–(V) Oxide Deposit, SW China. J. Petrol. 55, 951–976.

Liu, P.-P., Zhou, M.-F., Chen, W.T., Gao, J.-F., Huang, X.-W., 2014b. In-situ LA–ICP–MS trace elemental analyses of magnetite: Fe–Ti oxide-bearing intrusions of the Emeishan Large Igneous Province, SW China. Ore Geol. Rev. 65, 853–871.

Luan, Y., Song, X.-Y., Chen, L.-M., Zheng, W.-Q., Zhang, X.-Q., Yu, S.-Y., She, Y.-W., Tian, X.-L., Ran, Q.-Y., 2014. Key factors controlling the accumulation of the Fe–Ti oxides in the Hongge layered intrusion in the Emeishan Large Igneous Province, SW China. Ore Geol. Rev. 57, 518–538.

Ma, Y., Ji, X.-T., Li, J.-C., Huang, M., Kan, Z.-Z., 2003. Mineral Resources of the Panzhihua Region. Sichuan Science and Technology Press, Chengdu, p. 275 (in Chinese).

Nadoll, P., Angerer, T., Mauk, J.L., French, D., Walshe, J., 2014. The chemistry of hydrothermal magnetite: a review. Ore Geol. Rev. 61, 1–32.

Nadoll, P., Mauk, J.L., Hayes, T.S., Koenig, A.E., Box, S.E., 2012. Geochemistry of magnetite from hydrothermal ore deposits and host rocks of the Mesoproterozoic Belt Supergroup, United States. Econ. Geol. 107, 1275–1292.

Namur, O., Charlier, B., Toplis, M.J., Higgins, M.D., Liégeois, J.P., Vander Auwera, J., 2010. Crystallization sequence and magma chamber processes in the ferrobasaltic Sept Iles layered intrusion, Canada. J. Petrol. 51, 1203–1236.

Pang, K.-N., Li, C., Zhou, M.-F., Ripley, E.M., 2008. Abundant Fe–Ti oxide inclusions in olivine from the Panzhihua and Hongge layered intrusions, SW China: evidence for early saturation of Fe–Ti oxides in ferrobasaltic magma. Contrib. Miner. Petrol. 156, 307–321.

Pang, K.-N., Li, C., Zhou, M.-F., Ripley, E.M., 2009. Mineral compositional constraints on petrogenesis and oxide ore genesis of the late Permian Panzhihua layered gabbroic intrusion, SW China. Lithos 110, 199–214.

Pang, K.-N., Zhou, M.-F., Qi, L., Shellnutt, J.G., Wang, C.Y., Zhao, D., 2010. Flood basalt-related Fe–Ti oxide deposits in the Emeishan large igneous province, SW China. Lithos 119, 123–136.

Philpotts, A.R., 1967. Origin of certain iron-titanium oxide and apatite rocks. Econ. Geol. 62, 303–315.

Qi, L., Zhou, M.-F., 2008. Platinum-group elemental and Sr–Nd–Os isotopic geochemistry of Permian Emeishan flood basalts in Guizhou Province, SW China. Chem. Geol. 248, 83–103.

She, Y.-W., Yu, S.-Y., Song, X.-Y., Chen, L.-M., Zheng, W.-Q., Luan, Y., 2014a. The formation of P-rich Fe–Ti oxide ore layers in the Taihe layered intrusion, SW China: implications for magma-plumbing system process. Ore Geol. Rev. 57, 539–559.

She, Y.-W., Song, X.-Y., Yu, S.-Y., Chen, L.-M., Wei, Y., Zheng, W.-Q., 2014b. The compositions of magnetite and ilmenite of the Taihe layered intrusion, Sichuan Province. Constraints on the formation of the P-rich Fe–Ti oxide ores. Acta Petrologica Sinica 30, 1443–1456 (in Chinese with English abstract).

Shellnutt, J.G., Denyszyn, S., Mundil, R., 2012. Precise age determination of mafic and felsic intrusive rocks from the Permian Emeishan large igneous province (SW China). Gondwana Res. 22, 118–126.

Shellnutt, J.G., Wang, K.-L., Zellmer, G.F., Iizuka, Y., Jahn, B.-M., Pang, K.-N., Qi, L., Zhou, M.-F., 2011. Three Fe–Ti oxide ore-bearing gabbro-granitoid complexes in the Panxi region of the Emeishan large igneous province, SW China. Am. J. Sci. 311, 773–812.

Shellnutt, J.G., Jahn, B.-M., Dostal, J., 2010. Elemental and Sr–Nd isotope geochemistry of microgranular enclaves from peralkaline A-type granitic plutons of the Emeishan large igneous province, SW China. Lithos 119, 34–46.

Shellnutt, J.G., Jahn, B.-M., 2010. Formation of the Late Permian Panzhihua plutonic-hypabyssal-volcanic igneous complex: implications for the genesis of Fe–Ti oxide deposits and A-type granites of SW China. Earth Planet. Sci. Lett. 289, 509–519.

Shellnutt, J.G., Zhou, M.-F., Zellmer, G., 2009. The role of Fe–Ti oxide crystallization in the formation of A-type granitoids with implications for the Daly gap: an example from the Permian Baima igneous complex, SW China. Chem. Geol. 259, 204–217.

Shellnutt, J.G., 2014. The Emeishan large igneous province: a synthesis. Geosci. Front. 5, 369–394.

Shearer, C., Papike, J., Spilde, M., 2001. Trace-element partitioning between immiscible lunar melts: an example from naturally occurring lunar melt inclusions. Am. Mineral. 86, 238–246.

Sisson, T., Grove, T., 1993. Experimental investigations of the role of H_2O in calc-alkaline differentiation and subduction zone magmatism. Contrib. Miner. Petrol. 113, 143–166.

Song, X.-Y., Qi, H.-W., Hu, R.-Z., Chen, L.-M., Yu, S.-Y., Zhang, J.-F., 2013. Formation of thick stratiform Fe–Ti oxide layers in layered intrusion and frequent replenishment of fractionated mafic magma: evidence from the Panzhihua intrusion, SW China. Geochem. Geophys. Geosyst. 14, 712–732.

Song, X.-Y., Zhou, M.-F., Hou, Z.-Q., Cao, Z.-M., Wang, Y.-L., Li, Y., 2001. Geochemical constraints on the mantle source of the upper Permian Emeishan continental flood basalts, southwestern China. Int. Geol. Rev. 43, 213–225.

Song, X.-Y., Qi, H.-W., Robinson, P.T., Zhou, M.-F., Cao, Z.-M., Chen, L.-M., 2008. Melting of the subcontinental lithospheric mantle by the Emeishan mantle plume; evidence from the basal alkaline basalts in Dongchuan, Yunnan, Southwestern China. Lithos 100, 93–111.

Song, X.-Y., Keays, R.-R., Xiao, L., Qi, H.-W., Ihlenfeld, C., 2009. Platinum-group element geochemistry of the continental flood basalts in the central Emeisihan Large Igneous Province, SW China. Chem. Geol. 262, 246–261.

Tao, Y., Li, C., Song, X.-Y., Ripley, E.M., 2008. Mineralogical, petrological, and geochemical studies of the Limahe mafic-ultramatic intrusion and associated Ni–Cu sulfide ores, SW China. Miner. Deposita 43, 849–872.

Tollari, N., Toplis, M.J., Barnes, S.J., 2006. Predicting phosphate saturation in silicate magmas: an experimental study of the effects of melt composition and temperature. Geochim. Cosmochim. Acta 70, 1518–1536.

Tollari, N., Barnes, S.J., Cox, R.A., Nabil, H., 2008. Trace element concentrations in apatites from the Sept-Îles Intrusive Suite, Canada—implications for the genesis of nelsonites. Chem. Geol. 252, 180–190.

Toplis, M.J., Carroll, M.R., 1995. An experimental study of the influence of oxygen fugacity on Fe–Ti oxide stability, phase relations, and mineral-melt equilibria in Ferro-Basaltic systems. J. Petrol. 36, 1137–1170.

Toplis, M.J., Corgne, A., 2002. An experimental study of element partitioning between magnetite, clinopyroxene and iron-bearing silicate liquids with particular emphasis on vanadium. Contrib. Miner. Petrol. 144, 22–37.

Toplis, M.J., Libourel, G., Carroll, M.R., 1994. The role of phosphorus in crystallisation processes of basalt: an experimental study. Geochim. Cosmochim. Acta 58, 797–810.

VanTongeren, J.A., Mathez, E.A., 2012. Large-scale liquid immiscibility at the top of the Bushveld Complex, South Africa. Geology 40, 491–494.

Veksler, I.V., Dorfman, A.M., Borisov, A.A., Wirth, R., Dingwell, D.B., 2007. Liquid immiscibility and the evolution of basaltic magma. J. Petrol. 48, 2187–2210.

Veksler, I.V., Dorfman, A.M., Danyushevsky, L.V., Jakobsen, J.K., Dingwell, D.B., 2006. Immiscible silicate liquid partition coefficients: implications for crystal-melt element partitioning and basalt petrogenesis. Contrib. Miner. Petrol. 152, 685–702.

Visser, W., Van Groos, A.K., 1979. Effects of P_2O_5 and TiO_2 on liquid–liquid equilibria in the system K_2O–FeO–Al_2O_3–SiO_2. Am. J. Sci. 279, 970–988.

Wang, C.Y., Zhou, M.-F., 2013. New textural and mineralogical constraints on the origin of the Hongge Fe–Ti–V oxide deposit, SW China. Miner. Deposita 48, 787–798.

Watson, E.B., 1976. Two-liquid partition coefficients: experimental data and geochemical implications. Contrib. Miner. Petrol. 56, 119–134.

Xiao, L., Xu, Y.-G., Mei, H.-J., Zheng, Y.-F., He, B., Pirajno, F., 2004. Distinct mantle sources of low-Ti and high-Ti basalts from the western Emeishan large igneous province, SW China: implications for plume–lithosphere interaction. Earth Planet. Sci. Lett. 228, 525–546.

Xu, Y.-G., Chung, S.-L., Jahn, B.M., Wu, G., 2001. Petrologic and geochemical constraints on the petrogenesis of Permian–Triassic Emeishan flood basalts in southwestern China. Lithos 58, 145–168.

Zhang, X.-Q., Song, X.-Y., Chen, L.-M., Xie, W., Yu, S.-Y., Zheng, W.-Q., Deng, Y.-F., Zhang, J.-F., Gui, S.-G., 2012. Fractional crystallization and the formation of thick Fe–Ti–V oxide layers in the Baima layered intrusion, SW China. Ore Geol. Rev. 49, 96–108.

Zhang, Z.-C., Mahoney, J.J., Mao, J.-W., Wang, F.-S., 2006. Geochemistry of picritic and associated basalt flows of the western Emeishan flood basalt province, China. J. Petrol. 47, 1997–2019.

Zhang, Z.-C., Mao, J.-W., Saunders, A.D., Ai, Y., Li, Y., Zhao, L., 2009. Petrogenetic modeling of three mafic-ultramafic layered intrusions in the Emeishan large igneous province, SW China, based on isotopic and bulk chemical constraints. Lithos 113, 369–392.

Zhong, H., Zhou, X.-H., Zhou, M.-F., Sun, M., Liu, B.-G., 2002. Platinum-group element geochemistry of the Hongge Fe–V–Ti deposit in the Pan-Xi area, southwestern China. Miner. Deposita 37, 226–239.

Zhong, H., Zhu, W.-G., 2006. Geochronology of layered mafic intrusions from the Pan-Xi area in the Emeishan large igneous province, SW China. Miner. Deposita 41, 599–606.

Zhou, M.-F., Arndt, N.T., Malpas, J., Wang, C.Y., Kennedy, A.K., 2008. Two magma series and associated ore deposit types in the Permian Emeishan large igneous province, SW China. Lithos 103, 352–368.

Zhou, M.-F., Robinson, P.T., Lesher, C.M., Keays, R.R., Zhang, C.-J., Malpas, J., 2005. Geochemistry, petrogenesis and metallogenesis of the Panzhihua gabbroic layered intrusion and associated Fe–Ti–V oxide deposits, Sichuan Province, SW China. J. Petrol. 46, 2253–2280.

Zhou, M.-F., Yan, D.-P., Kennedy, A.K., Li, Y., Ding, J., 2002. SHRIMP U–Pb zircon geochronological and geochemical evidence for Neoproterozoic arc-magmatism along the western margin of the Yangtze Block, South China. Earth Planet. Sci. Lett. 196, 51–67.